



Article

# Effects of Aqueous Dispersions of C<sub>60</sub>, C<sub>70</sub> and Gd@C<sub>82</sub> Fullerenes on Genes Involved in Oxidative Stress and Anti-Inflammatory Pathways

Elena V. Proskurnina <sup>1,\*</sup> , Ivan V. Mikheev <sup>2</sup> , Ekaterina A. Savinova <sup>1</sup>, Elizaveta S. Ershova <sup>1,3</sup>, Natalia N. Veiko <sup>1</sup>, Larisa V. Kameneva <sup>1</sup>, Olga A. Dolgikh <sup>1</sup> , Ivan V. Rodionov <sup>3</sup>, Mikhail A. Proskurnin <sup>2</sup> and Svetlana V. Kostyuk <sup>1,3</sup>

<sup>1</sup> Laboratory of Molecular Biology, Research Centre for Medical Genetics, 1 Moskvorechye St, 115522 Moscow, Russia; savinova.ekaterina96@yandex.ru (E.A.S.); es-ershova@rambler.ru (E.S.E.); satelit32006@yandex.ru (N.N.V.); kamlar@med-gen.ru (L.V.K.); dolgiko@med-gen.ru (O.A.D.); svet-vk@yandex.ru (S.V.K.)

<sup>2</sup> Department of Chemistry, Lomonosov Moscow State University, 1-3 Leninskie Gory, 119991 Moscow, Russia; mikheev.ivan@gmail.com (I.V.M.); proskurnin@gmail.com (M.A.P.)

<sup>3</sup> Department of Normal Physiology, I.M. Sechenov First Moscow State Medical University (Sechenov University), 11-5 Mokhovaya St, 125007 Moscow, Russia; vano121099@mail.ru

\* Correspondence: proskurnina@gmail.com



**Citation:** Proskurnina, E.V.; Mikheev, I.V.; Savinova, E.A.; Ershova, E.S.; Veiko, N.N.; Kameneva, L.V.; Dolgikh, O.A.; Rodionov, I.V.; Proskurnin, M.A.; Kostyuk, S.V. Effects of Aqueous Dispersions of C<sub>60</sub>, C<sub>70</sub> and Gd@C<sub>82</sub> Fullerenes on Genes Involved in Oxidative Stress and Anti-Inflammatory Pathways. *Int. J. Mol. Sci.* **2021**, *22*, 6130. <https://doi.org/10.3390/ijms22116130>

Academic Editor: Maria Giulia Lionetto

Received: 2 May 2021  
Accepted: 5 June 2021  
Published: 7 June 2021

**Publisher's Note:** MDPI stays neutral with regard to jurisdictional claims in published maps and institutional affiliations.



**Copyright:** © 2021 by the authors. Licensee MDPI, Basel, Switzerland. This article is an open access article distributed under the terms and conditions of the Creative Commons Attribution (CC BY) license (<https://creativecommons.org/licenses/by/4.0/>).

**Abstract:** Background: Fullerenes and metallofullerenes can be considered promising nanopharmaceuticals themselves and as a basis for chemical modification. As reactive oxygen species homeostasis plays a vital role in cells, the study of their effect on genes involved in oxidative stress and anti-inflammatory responses are of particular importance. Methods: Human fetal lung fibroblasts were incubated with aqueous dispersions of C<sub>60</sub>, C<sub>70</sub>, and Gd@C<sub>82</sub> in concentrations of 5 nM and 1.5 μM for 1, 3, 24, and 72 h. Cell viability, intracellular ROS, NOX4, NFκB, PRAR-γ, NRF2, heme oxygenase 1, and NAD(P)H quinone dehydrogenase 1 expression have been studied. Results & conclusion: The aqueous dispersions of C<sub>60</sub>, C<sub>70</sub>, and Gd@C<sub>82</sub> fullerenes are active participants in reactive oxygen species (ROS) homeostasis. Low and high concentrations of aqueous fullerene dispersions (AFD) have similar effects. C<sub>70</sub> was the most inert substance, C<sub>60</sub> was the most active substance. All AFDs have both “prooxidant” and “antioxidant” effects but with a different balance. Gd@C<sub>82</sub> was a substance with more pronounced antioxidant and anti-inflammatory properties, while C<sub>70</sub> had more pronounced “prooxidant” properties.

**Keywords:** aqueous fullerene dispersions; pristine fullerenes; metallofullerenes; ROS homeostasis; oxidative stress; NOX4; Nrf2; PRAR-γ; heme oxygenase 1; NAD(P)H quinone dehydrogenase 1; anti-inflammatory pathways

## 1. Introduction

Nanomaterials are being increasingly used in medicine. According to the PubMed database, there are more than 3500 reviews related to the terms “nanoparticles” or “nanomedicine” in article titles over the past five years. Fullerenes are increasingly being used in various biomedical fields owing to their unique, size-dependent functions and physicochemical properties [1–3]. The possibility of modifying the surface of fullerenes [4] and incorporating heteroatoms into a carbon cage (endohedral fullerenes) [5] opens up prospects for synthesizing substances with targeted biochemical properties. Thus, fullerenes and their derivatives are used as drug-delivery systems for anticancer therapy [6], antimicrobial agents [7], and antiviral agents [7]. Among metallofullerenes, gadolinium-containing endohedral fullerenes represent a new class of effective relaxation agents for magnetic resonance imaging (MRI) [8].

Fullerenes are efficient antioxidants ( $C_{60}$  is even called a “free radical sponge”) [9,10], which allows them to be considered neuroprotective [11], anti-inflammatory, and anti-ischemic [12] agents. When applied topically,  $C_{60}$  and its derivatives were used to treat cartilage degeneration, bone destruction, intervertebral disc degeneration, vertebral bone marrow disorder, and radiculopathy [13]. Antioxidant effects of water-soluble carboxyfullerene have been proved in vivo [14]. The possibility of fullerenes acting as mitochondria protonophores allows them to be considered anti-aging antioxidants [15,16]. Hydroxylated  $Gd@C_{82}$  has antineoplastic activity simultaneously with low toxicity [17,18].

Reactive oxygen species (ROS) homeostasis is a complex metabolic system, which involves many sources of ROS, the activity of which depends on the expression of the respective genes. The most important enzymes of ROS homeostasis are NADPH oxidases, respiratory chains of mitochondria and endoplasmic reticulum, peroxidases, catalase, superoxide dismutase, and others. ROS homeostasis is closely related to inflammation, carcinogenesis, apoptosis, and cell proliferation. Several proinflammatory and anti-inflammatory signaling pathways are ROS-dependent. Therefore, studying the role of fullerenes in ROS homeostasis should include research on the effect of fullerenes on signaling pathways and gene expression.

Several studies were devoted to the effect of fullerenes on genes, primarily from the point of view of toxicity. Fullerene  $C_{60}$  derivatives cause the activation of several genes in cells [19,20], and the cell response depends on the functional groups of the fullerene. Studying the gene expression in rat lungs after whole-body inhalation exposure to  $C_{60}$  fullerene revealed that few genes involved in the inflammatory response, oxidative stress, apoptosis, and metalloendopeptidase activity were upregulated at both three days and a month post-exposure. Some genes associated with the immune system process, including major histocompatibility complex-mediated immunity, were upregulated [21]. The exposure to hydroxylated fullerenes caused shifts in gene regulation involved in circadian rhythm, kinase activity, vesicular transport, and immune response [22]. A water-soluble pyrrolidinium fullerene derivative,  $C_{60}$ -bis (N, N-dimethylpyrrolidinium iodide), markedly induced apoptosis of JAK2 V617F mutant-induced transformed cells through a novel mechanism, inhibiting c-Jun N-terminal kinase (JNK) activation pathway [23]. Administration of  $C_{60}HyFn$  in HHcy mice significantly reduces the serum homocysteine level, neuronal apoptosis, and the expression level of the TRPM2 gene [24].  $C_{60}(OH)_{24}$  may attenuate oxidative stress-induced apoptosis via augmentation of Nrf2-regulated cellular antioxidant capacity, thus providing insights into the mechanisms of antioxidant properties of  $C_{60}(OH)_{24}$  [25]. Fullerenes mediate proliferation and cardiomyogenic differentiation of adipose-derived stem cells via the modulation of MAPK pathway and cardiac protein expression [26]. Fullerenols (hydroxylated fullerenes) inhibit the crosstalk between bone marrow-derived mesenchymal stem cells and tumor cells by regulating MAPK signaling [27].

For biological applications, the surface of fullerenes should be hydrophilized by, for example, hydroxylation [28]. Fullerenols have pronounced antioxidant activity with relatively low toxicity [29]. Moreover, pristine fullerenes can form stable hydrophilic  $nC_{60}$  aggregates in water [30]. Previously, we reported on a green, scalable, and sustainable approach to preparing aqueous fullerene dispersions (AFD) of  $C_{60}$ ,  $C_{70}$ , and  $Gd@C_{82}$  and their derivatives using sonication with an immersed ultrasonic probe [31]. Despite the apparent advantages of aqueous dispersions of pristine fullerenes, their biochemical properties have been studied exceptionally poorly. AFD stimulated the natural heterotrophic bacterioplankton and inhibited the bactericidal activity of antibiotics [32]. We have shown that AFDs of  $C_{60}$ ,  $C_{70}$ , and  $C_{82}$  are moderate scavengers of superoxide anion radicals [33]. We failed to find systemic studies on the effect of aqueous dispersions of pristine fullerenes and endohedral fullerenes on the oxidative stress in cells and the cell cycle.

Here, we have studied the effects of the aqueous dispersions of  $C_{60}$ ,  $C_{70}$ , and  $Gd@C_{82}$  on ROS homeostasis in human fetal lung fibroblasts concerning: (1) cell toxicity, (2) intracellular ROS, (3) NOX4 regulation, (4) NRF2 pathway modulation, (5) NF $\kappa$ B pathway

modulation, and (6) expression of heme oxygenase 1 and NAD(P)H quinone dehydrogenase 1.

## 2. Results

### 2.1. Preparation and Characterization of Aqueous Fullerene Dispersions

AFDs have been prepared by direct ultrasound sonication of pristine C<sub>60</sub>, C<sub>70</sub>, and Gd@C<sub>82</sub> (C<sub>2v</sub>) in ultrapure water. The direct sonication procedure without solubilizing agents was previously developed to synthesize fullerene derivatives [34]. We used an immersion ultrasound probe made of titanium. Despite the formation of titania nanoparticles during ultrasonication, this procedure produces efficiently dispersed nanoparticles [35,36]. According to ICP–OES, a prolonged ultrasound exposure of fullerene C<sub>60</sub>–water mixtures resulted in the concentration of total titanium as low as 3.50 ± 0.05 ppm. Cellulose syringe filters with a pore diameter of 0.45 and 0.22 μm were used to purify the dispersions from titanium. As a result, all the prepared samples contained less than 1 ppm titanium dioxide.

The sizes of colloidal particles in AFDs estimated by dynamic light scattering (DLS) are in the range 90–115 nm. The DLS profiles are shown in Figure S1 in the Supplementary Materials. Fullerene clusters were negatively charged with zeta potentials about −30 mV, which characterizes AFDs as stable colloidal systems.

The polydispersity index (PDI) characterizes the mono- or polydispersity of colloidal systems. According to ISO 22412: 2008, the polydispersity index is usually less than 0.1 for monodisperse samples. For C<sub>60</sub>, the PDI value was 0.109, which indicates a slight agglomeration and deviation from the monodispersity. For C<sub>70</sub>, the PDI is 0.160, which may indicate a significant difference in the structure of the clusters. The PDI for Gd@C<sub>82</sub> is between the PDI values for C<sub>60</sub> and C<sub>70</sub>.

The details of the prepared samples are presented in Table 1.

**Table 1.** Concentrations (c), size, zeta-potentials (ζ), and polydispersity indices (PDI) of the AFDs.

Fullerene	c, mM	Particle Size after a 0.22 μm Filter, nm	ζ-potential, mV	PDI
C <sub>60</sub>	0.083 <sup>1</sup>	110 ± 5	−28.4 ± 0.2	0.109 ± 0.003
C <sub>70</sub>	0.081 <sup>1</sup>	113 ± 2	−29.5 ± 0.3	0.160 ± 0.008
Gd@C <sub>82</sub>	0.022 <sup>2</sup>	95 ± 5	−32.3 ± 0.3	0.123 ± 0.008

<sup>1</sup> Measured by UV/vis spectroscopy. <sup>2</sup> Measured by ICP–OES.

Photographs of the aqueous fullerene dispersions are presented in Figure S2, and TEM images are presented in Figure S3 in the Supplementary Materials. The average cluster size assessed with TEM was approximately 100 nm that correlates sufficiently with the data obtained with dynamic light scattering.

The purity of the obtained AFDs was checked by the MALDI method. All the spectra contain an intense molecular ion M and adducts of M with C<sub>2</sub> (M + 24n) (Figure 1). The spectra show no signs of fullerene modification. The presence of adducts in the mass spectra can be explained by the coalescence phenomenon [37].

Surface functional groups were assessed by Fourier-transform infrared spectroscopy (FTIR). FTIR spectra are presented in Figure S4 in the Supplementary Materials. Main fullerene bands are present in all FTIR spectra with no bands indicating significant modifications of the fullerene surface. To improve water evaporation, we increased the diamond ATR crystal temperature up to 50 °C. For C<sub>60</sub>, we have observed main bands at 526, 578, 1180, and 1428 cm<sup>−1</sup> which are characteristic for C<sub>60</sub> [38]. There were no bands related to OH- or epoxy groups as reported in [39]. For C<sub>70</sub>, the main bands were as follows: 1429, 1173, 1134, 793, 723, 674, 578, 535, 457 cm<sup>−1</sup> which agrees with the previously obtained data [38,40].

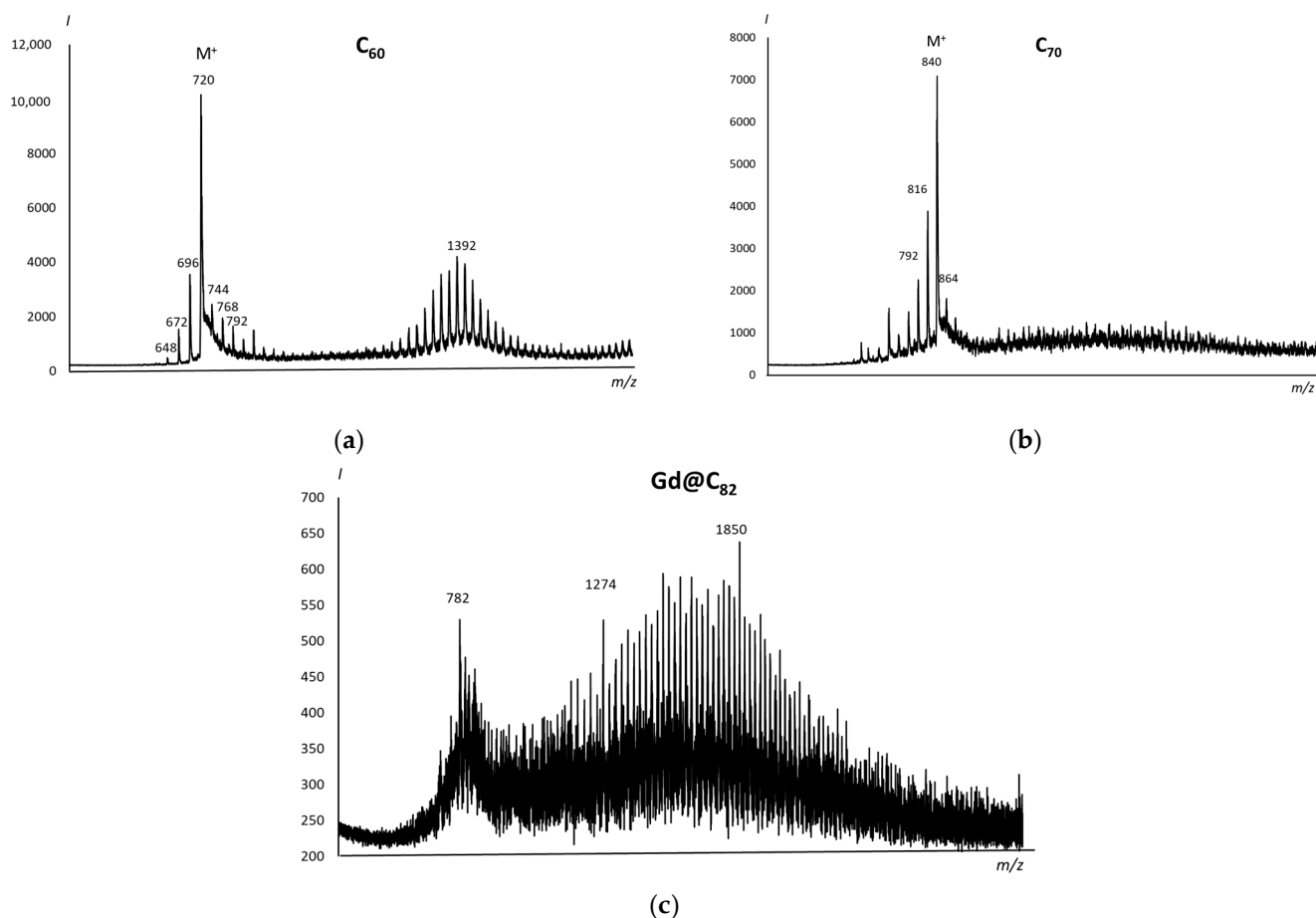


**Figure 1.** MALDI positive-ion mass spectra of AFDs of (a)  $C_{60}$ , (b) ( $C_{70}$ ), and (c)  $Gd@C_{82}$  in an  $\alpha$ -cyano-4-hydroxycinnamic acid matrix.

Due to the low IR absorption and a large number of absorption bands, we could not register a resolved FTIR spectrum for  $Gd@C_{82}$ . Characteristic IR bands at 1116, 1022 and  $995\text{ cm}^{-1}$  were not resolved and only  $1063\text{ cm}^{-1}$  resolved band was observed [41]. Just like for  $C_{60}$  and  $C_{70}$ , there were no bands related to OH- or epoxy groups.

## 2.2. Cell Viability

Cell viability was examined by a conventional MTT assay. Aqueous dispersions of  $C_{60}$ ,  $C_{70}$ , and  $Gd@C_{82}$  were studied in a wide concentration range from 15 pM to 8.2  $\mu\text{M}$ , from 15 pM to 9.1  $\mu\text{M}$ , and from 0.2 pM to 105 nM, respectively. The fullerenes were incubated with cells for 72 h.

For all studied concentrations, the aqueous dispersion of  $C_{60}$  did not have toxic effects on cells and only at 8.2  $\mu\text{M}$  decreased cell viability by 20% (Figure 2a). The aqueous dispersion of  $C_{70}$  decreased cell viability by less than 20% at 15 pM–1.4 nM concentrations. Interesting in concentrations of 1.4 nM–9.1  $\mu\text{M}$ ,  $C_{70}$  stimulated cells. Cell viability increased approx. at 20% (Figure 2b). Adding  $Gd@C_{82}$  was the least favorable for cells. Starting from 0.9 pM, this compound decreased cell viability by 20% (Figure 2c). To sum,  $C_{60}$  and  $C_{70}$  AFDs were non-toxic in concentrations less than 9  $\mu\text{M}$  and  $Gd@C_{82}$  was non-toxic in concentrations less than 0.1  $\mu\text{M}$ .

## 2.3. Mitochondrial Potential

The MTT test is commonly used to assess cellular metabolic activity, mainly to assess mitochondrial functionality. Next, we analyzed the response of HFLF mitochondria to the addition of AFDs. Using flow cytometry, we found that the intensity of the TMRM signal in the mitochondria increased by a factor of 2.4 after 1 h of incubation with 1.5  $\mu\text{M}$

C<sub>60</sub>. After 3 h of incubation, the signal level returned to the blank values. After 24 h of incubation, we observed a slight increase in the signal level. In concentrations of 5 nM, C<sub>60</sub> did not significantly affect the mitochondrial potential (Figure 3a).

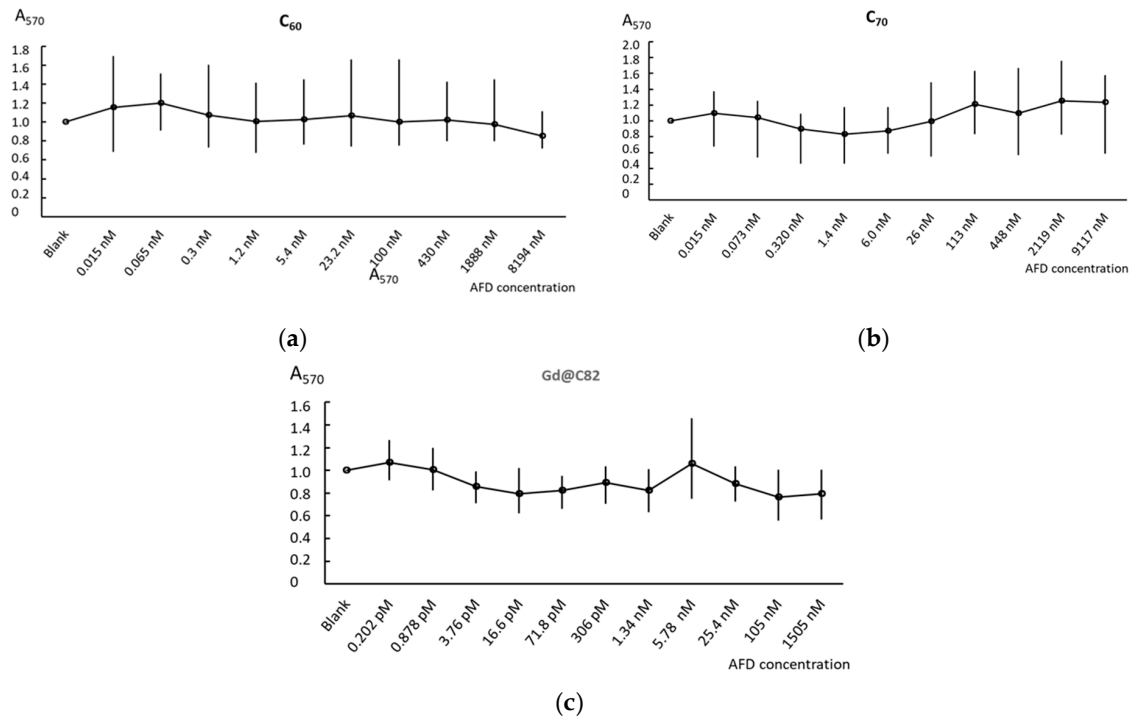


**Figure 2.** The MTT test: cell viability in versus concentrations of C<sub>60</sub> (a), C<sub>70</sub> (b), and Gd@C<sub>82</sub> (c) after 72 h of incubation. In blank experiments, cells were incubated without the AFDs.

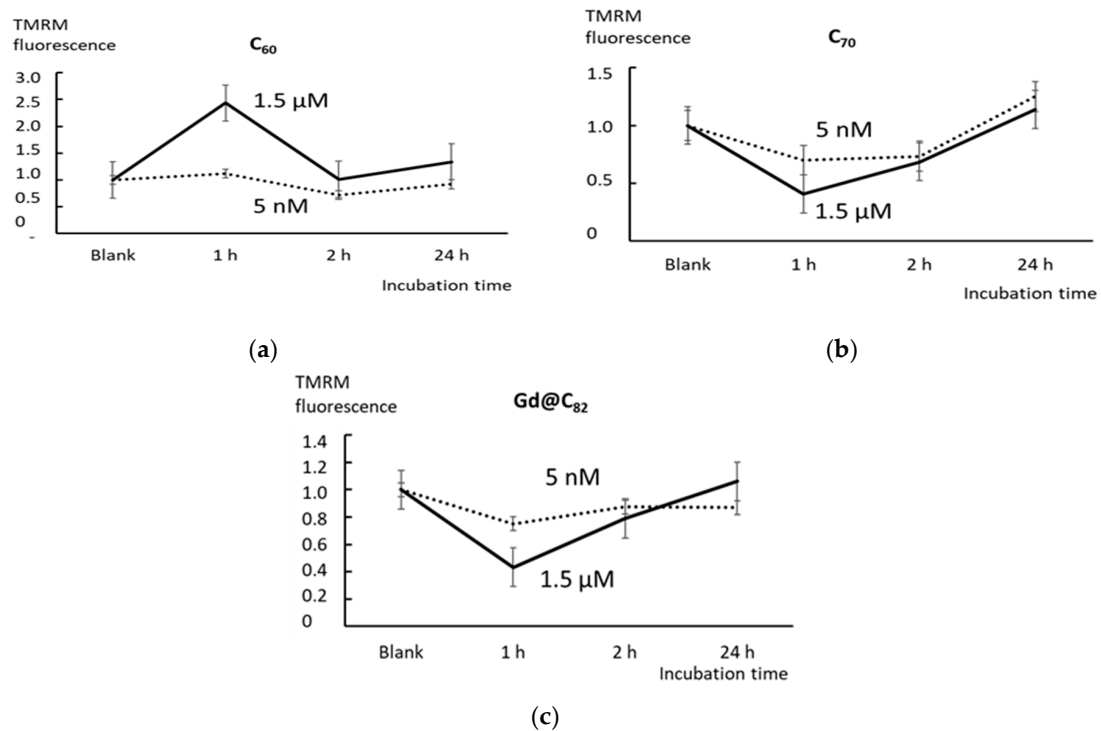


**Figure 3.** The mitotracker test with TMRM using flow cytometry: the relative enhancement of the mitotracker signal in cells relative to the blank versus incubation time with C<sub>60</sub> (a), C<sub>70</sub> (b), and Gd@C<sub>82</sub> (c). In blank experiments, cells were incubated without AFDs. Concentrations are indicated in the figure.

Fullerene  $C_{70}$  (both 5 nM and 1.5  $\mu$ M) and  $Gd@C_{82}$  (1.5  $\mu$ M) after 1 h of incubation decreased the mitochondrial potential. After 3 h of incubation, the mitochondrial potential increased. After 24 h of incubation, the mitochondrial potential reached blank values.  $Cd@C_{82}$  at a concentration of 5 nM did not have a statistically significant effect on the mitochondrial potential (Figure 3b,c).

Decreasing the TMRM signal in cells can be caused by two processes. The first cause is quenching the mitotracker by fullerene; the second is capturing energy by  $C_{70}$  and  $Gd@C_{82}$  from the TMRM dye. These processes can occur given the close contact of fullerene molecules with a mitotracker provided in mitochondria. This conclusion is confirmed by several studies on the localization of fullerenes in mitochondria [42,43].

#### 2.4. Localization of Fullerenes inside Human Fetal Lung Fibroblasts

To study the penetration and distribution of the fullerenes in cells, fluorescence imaging was registered. Fluorescence images of cells incubated for 3 and 24 h with  $C_{60}$ ,  $C_{70}$ , and  $Gd@C_{82}$  are shown in Figures 4–6, respectively.

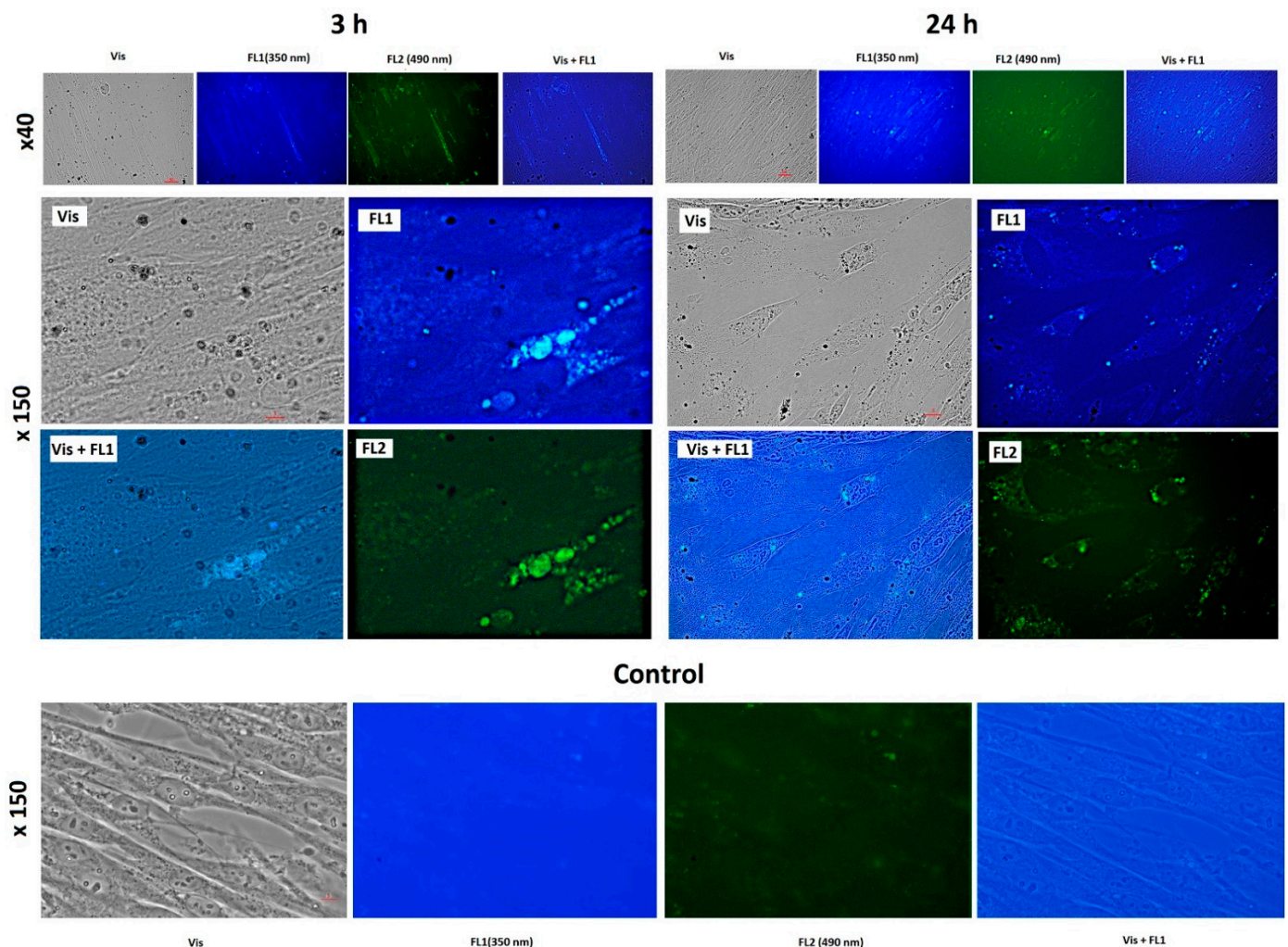


**Figure 4.** Fluorescence of  $C_{60}$  (concentration 1.5  $\mu$ M) in the cells after 3 and 24 h of incubation: Vis, transmitted light, fluorescence was registered with a 450–525 nm filter, excitation wavelength 350 nm (FL1) and 490 (FL2); magnification is shown at the left. Scale is marked with red bars. The bottom series of photographs are images of cells incubated without the fullerene (a control experiment).

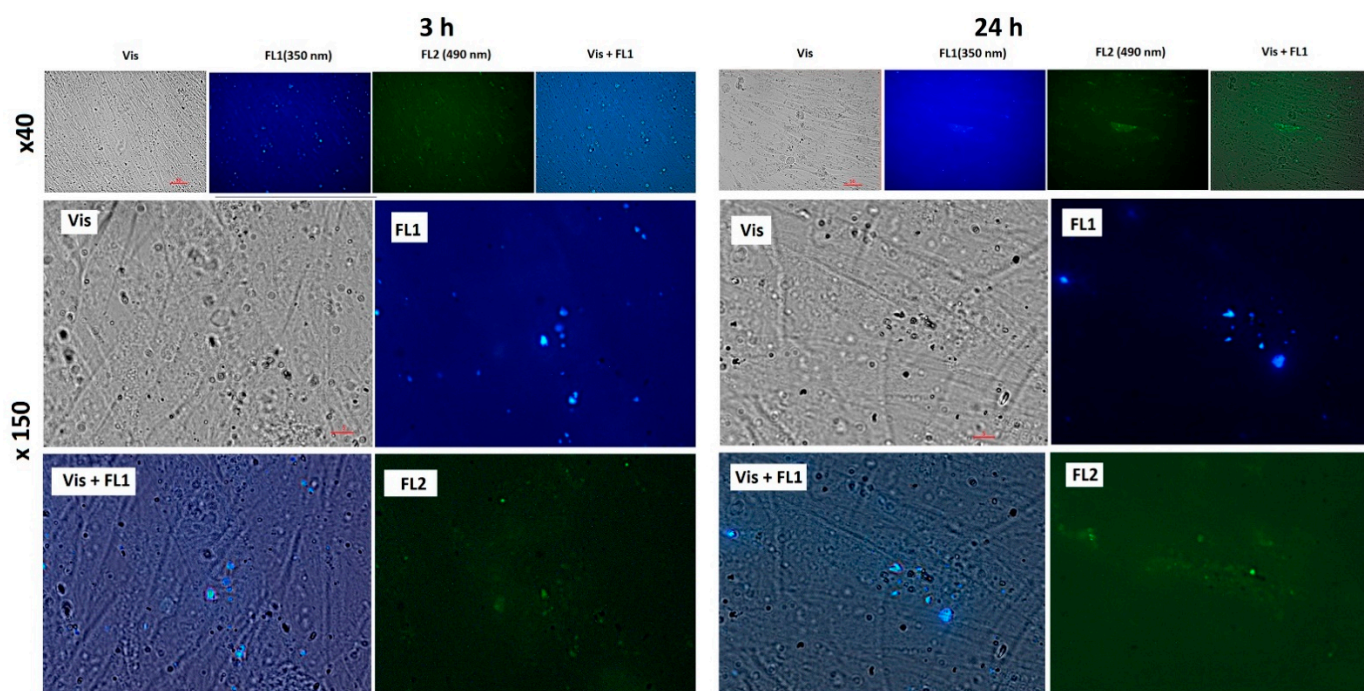


**Figure 5.** Fluorescence of  $C_{72}$  (concentration  $1.5 \mu\text{M}$ ) in the cells after 3 and 24 h of incubation: Vis, transmitted light, fluorescence was registered with a 450–525 nm filter, excitation wavelength 350 nm (FL1) and 490 (FL2); magnification is shown at the left. Scale is marked with red bars.

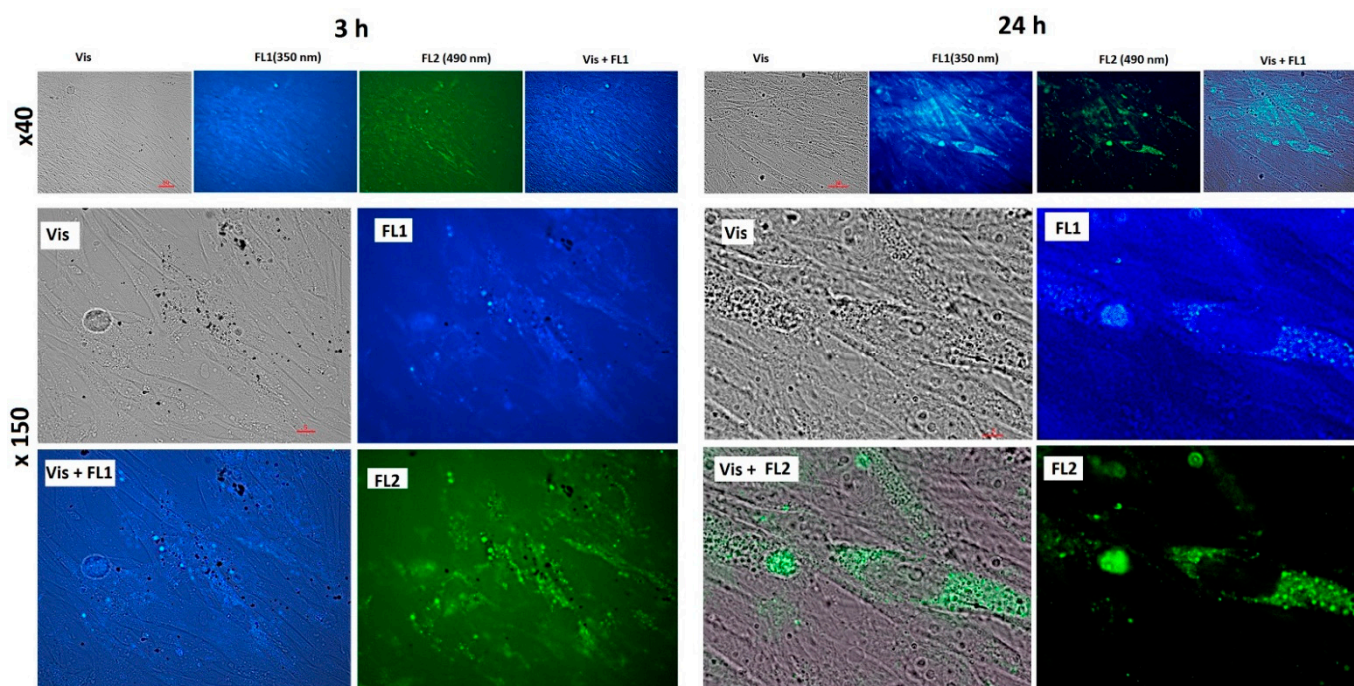


**Figure 6.** Fluorescence of  $Gd@C_{82}$  (concentration  $1.5 \mu\text{M}$ ) in the cells after 3 and 24 h of incubation: Vis—transmitted light, fluorescence was registered with a 450–525 nm filter, excitation wavelength 350 nm (FL1) and 490 (FL2); magnification is shown at the left. Scale is marked with red bars.

The photographs show that after 3 h of incubation, the fullerenes are localized mainly at the cell surface. The absorption of fullerenes was not strong as they were washed off during washing. After 24 h, fullerenes penetrate the cell membrane into the cytoplasm.

The photographs clearly show dark rounded nuclei, into which fullerenes do not penetrate. The results of flow cytometry confirm the data of fluorescence microscopy.

### 2.5. Intracellular ROS

After incubation with AFDs, intracellular ROS were detected with H2DCFH-DA (2,7-dichlorodihydrofluorescein diacetate) using a flow cytometer. After permeation into a cell, the compound is deacetylated with intracellular esterases. Free radicals oxidize the nonfluorescent H2DCFH in the cytoplasm to the highly fluorescent 2',7'-dichlorofluorescein. Figure 4 shows the histograms of DCF production in the cells after adding C<sub>60</sub>, C<sub>70</sub>, and Gd@C<sub>82</sub> related to blank cells versus the incubation time.

C<sub>60</sub> added to the cells tends to decrease the ROS level in cells after 1 and 3 h regardless of the concentration. Intracellular ROS is lowered despite the high activity of the NOX4 enzyme (see below, Section 2.6) and mitochondria, which promote ROS synthesis. After 24 h of incubation, the ROS level increased above the control values (Figure 7a).

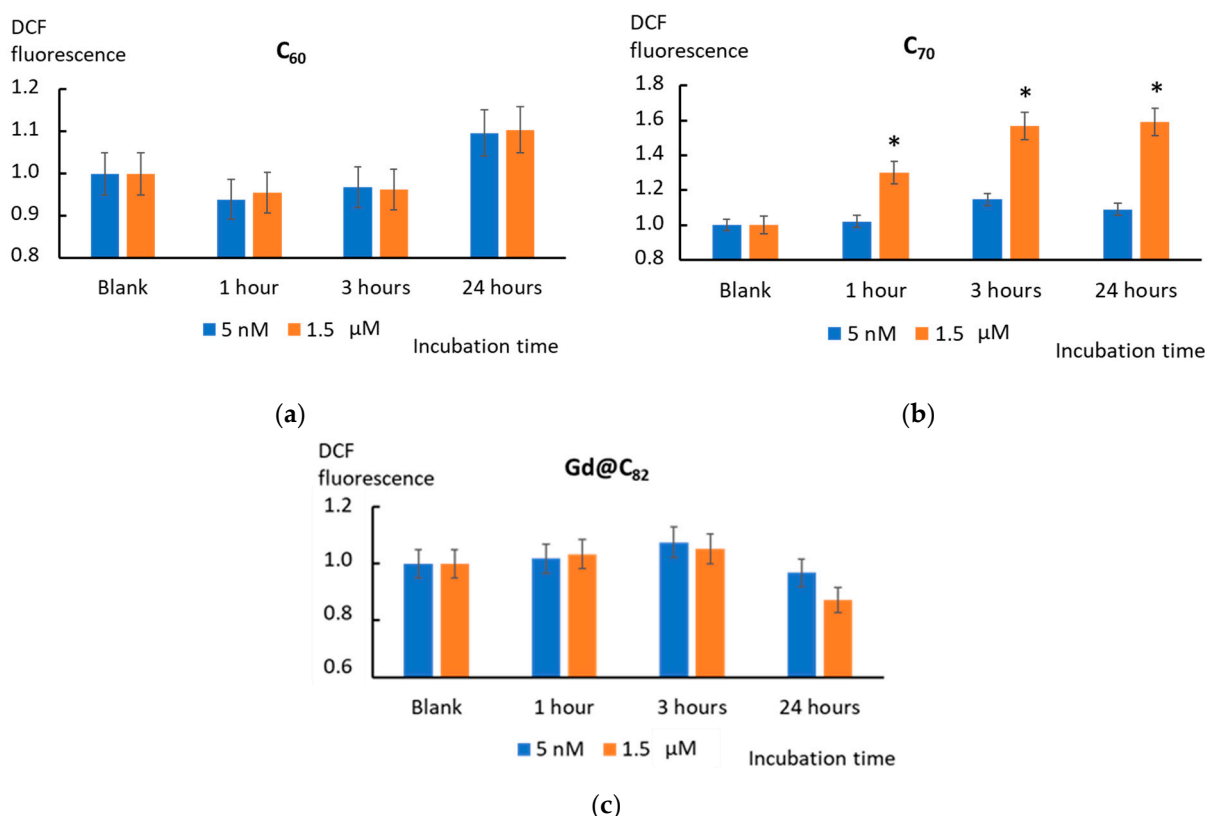


**Figure 7.** The histograms of intracellular ROS production on the incubation time for C<sub>60</sub> (a), C<sub>70</sub> (b), and Gd@C<sub>82</sub> (c) at the concentrations of 5 nM and 1.5 μM; flow cytometry was used. (\*) denotes significant differences with the blank cells,  $p < 0.01$ , a nonparametric U-test.

Incubation with C<sub>70</sub> (1.5 μM) caused a significant increase in the ROS level ( $p < 0.01$ ) after 1, 3, and 24 h incubations. At a nanomolar concentration (5 nM), the ROS level did not increase significantly (Figure 7b).

Incubation with Gd@C<sub>82</sub> resulted in a slightly increased ROS level after 3 h of incubation. After 24 h, a decrease in the ROS level was observed, specially marked for micromolar concentrations (Figure 7c).

### 2.6. NOX4 Expression

One of the primary sources of ROS in cells is NADPH oxidases (NOX), which are predominantly localized in endosomes [44]. We studied the expression of the NOX4 gene and protein in the cells following their incubation with AFDs of C<sub>60</sub>, C<sub>70</sub>, and Gd@C<sub>82</sub>.

For 1.5  $\mu\text{M}$   $\text{C}_{60}$ , the NOX4 protein level increased by three ( $p < 0.01$ ) after 1 h of incubation and remained increased by a factor of 1.5–2.8 within 3–24 h. After 72 h of incubation, NOX4 protein decreased to a lower value than the blank. At a concentration of 5 nM,  $\text{C}_{60}$  caused an increase in NOX4 after 24 h of incubation by a factor of two ( $p < 0.01$ ). The NOX 4 protein decreased below the blank after 72 h of incubation (Figure 8a). For 1.5  $\mu\text{M}$   $\text{C}_{70}$ , the NOX4 protein level increased by a factor of 1.6–1.4 ( $p < 0.01$ ) within 3–24 h and decreased to a value lower than the blank by 40% ( $p < 0.01$ ) after 72 h of incubation. At a concentration of 5 nM,  $\text{C}_{70}$  did not cause significant changes in NOX4 protein expression within 72 h of incubation (Figure 8c). Fullerene  $\text{Gd@C}_{82}$  only at a concentration of 1.5  $\mu\text{M}$  caused an increase in the NOX4 level after 24 h of incubation by a factor of 2.5 ( $p < 0.01$ ) and an almost twofold decrease ( $p < 0.01$ ) below the blank values after 72 h (Figure 8d).

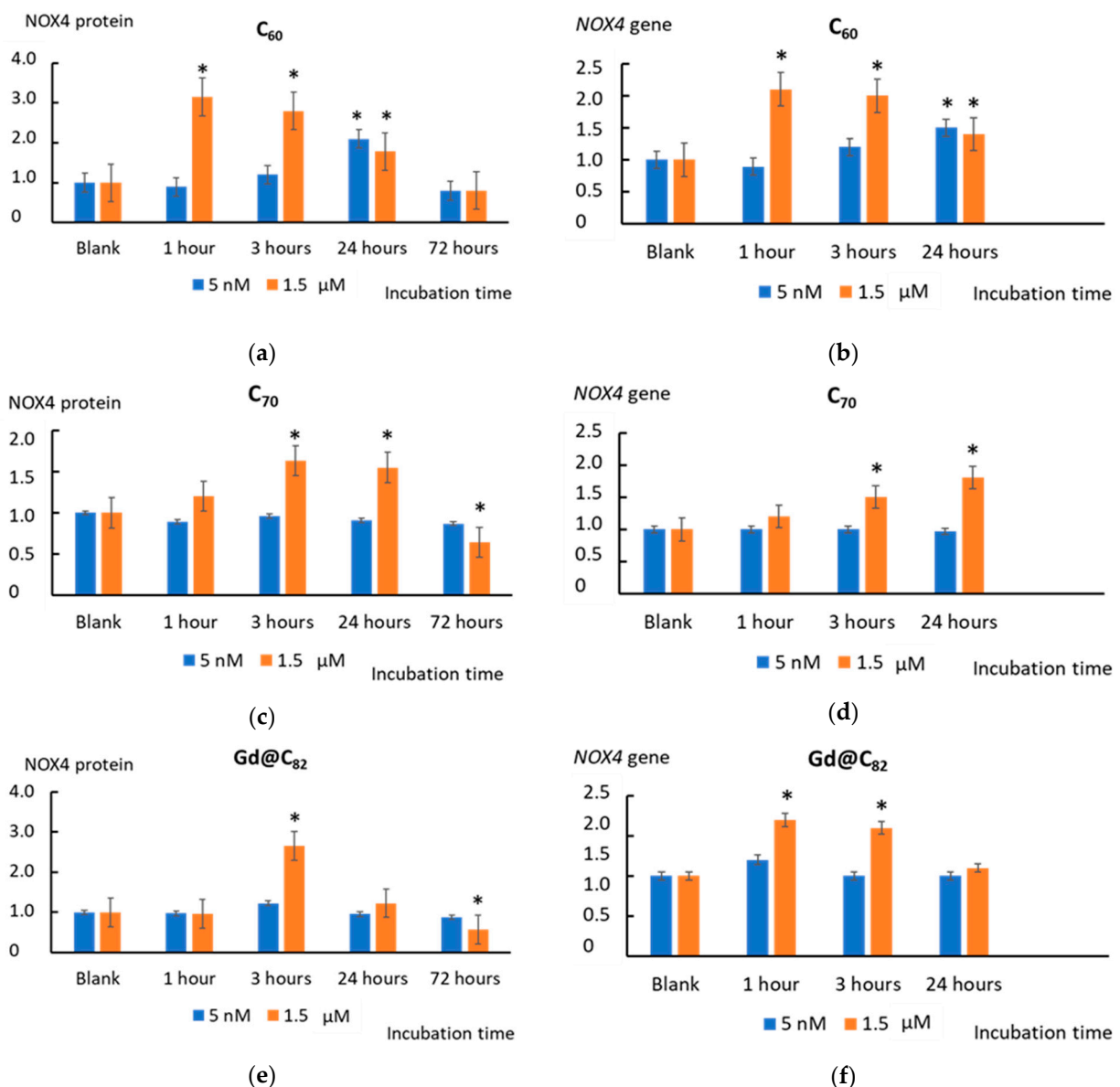


**Figure 8.** The NOX4 protein level in cells treated with (a)  $\text{C}_{60}$ , (c)  $\text{C}_{70}$ , and (e)  $\text{Gd@C}_{82}$  at the concentrations of 5 nM and 1.5  $\mu\text{M}$ . The expression of the NOX4 gene in cells incubated with (b)  $\text{C}_{60}$ , (d)  $\text{C}_{70}$ , and (f)  $\text{Gd@C}_{82}$  at the concentration of 5 nM and 1.5  $\mu\text{M}$ . The NOX4 RNA level is the mean from three replicates related to the NOX4 gene expression in the blank cells. The *TBP* gene was used as an internal-standard gene. The blank cells were incubated without the AFDs. (\*) denotes significant differences with the blank cells,  $p < 0.01$ , a nonparametric U-test.

NOX4 expression is regulated by its transcription. The NOX4 protein level and NOX4 gene transcriptional activity changes agreed. The NOX4 transcription caused by the studied fullerenes changed synchronously with the change in the protein expression level, but slightly ahead of time (Figure 8b,d,f).

### 2.7. NFκB Pathway and PPAR-γ

We have not found effects of C<sub>60</sub>, C<sub>70</sub>, and Gd@C<sub>82</sub> on the NFκB pathway either for the expression of *NFKB1* gene or for the NFκB transcription factor. We also have not found any effects on the expression of target genes of NFκB pathway such as *TNFA*, *IL-6*, and *IL-1B*.

The peroxisome proliferator-activated receptor-γ (PPAR-γ) is involved in the antioxidant response. It inhibits the NFκB signaling pathway, which leads to a decrease in the expression of proinflammatory mediator genes [45,46]. C<sub>60</sub> (1.5 μM) increased PPAR-γ expression after 24 h of incubation. C<sub>60</sub> (5 nM) increased the PPAR-γ expression after 1 h of incubation by a factor of 2.5 ( $p < 0.01$ ) (Figure 9a). Fullerenes C<sub>70</sub> and Gd@C<sub>82</sub> caused an increase in PPAR-γ expression by a factor of 1.4–1.8 after 72 h of incubation ( $p < 0.01$ ) (Figure 9b,c).

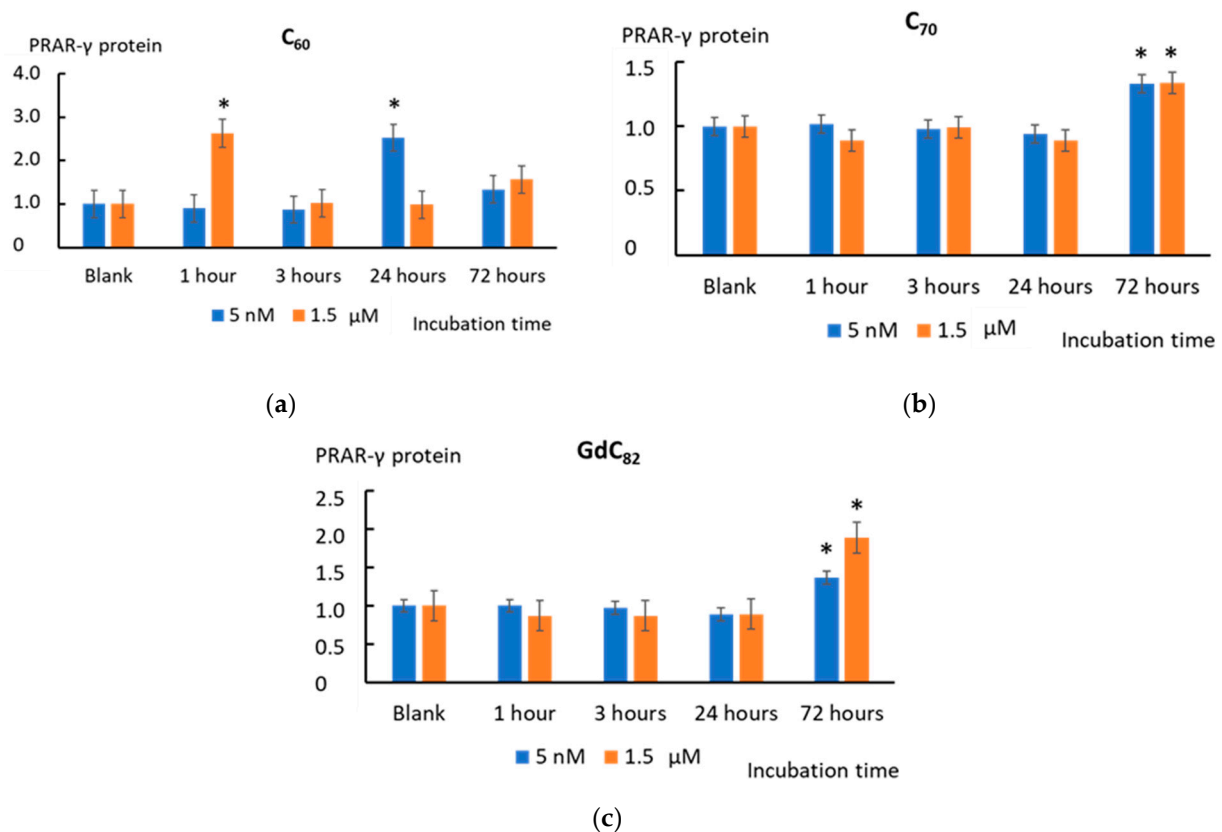


**Figure 9.** The PRAR-γ protein level in cells treated with (a) C<sub>60</sub>, (b) C<sub>70</sub>, and (c) Gd@C<sub>82</sub> at concentrations of 5 nM and 1.5 μM. The blank cells were incubated without the AFDs. (\*) denotes significant differences with the blank cells,  $p < 0.01$ , a nonparametric U-test.

### 2.8. NRF2 Pathway

Cellular ROS are regulated by ROS production systems and antioxidant response systems such as the transcription factor NRF2, a component of the anti-inflammatory pathway.

The expression of NRF2 protein increased by a factor of 1.5–1.8 after 1 h of incubation with all the studied AFDs both in nanomolar and micromolar concentrations (except for 5 nM C<sub>60</sub>). After 3 h of incubation with C<sub>60</sub> and C<sub>70</sub>, the NRF2 expression did not change. AFD Gd@C<sub>82</sub> slightly increased the NRF2 expression (Figure 10). After 24 h, the NRF2

expression in the cells incubated with  $C_{60}$  for both concentrations increased by 30–50% and gradually decreased in 72 h (Figure 10a). AFD  $C_{70}$  did not affect the NRF2 expression after 24 or 72 h (Figure 10c). After 24 h,  $Gd@C_{82}$  in micromolar concentration caused an increase in the NRF2 level by a factor of 1.8 ( $p < 0.01$ ). After 72 h of incubation, the NRF2 expression decreased to the blank values (Figure 10e).

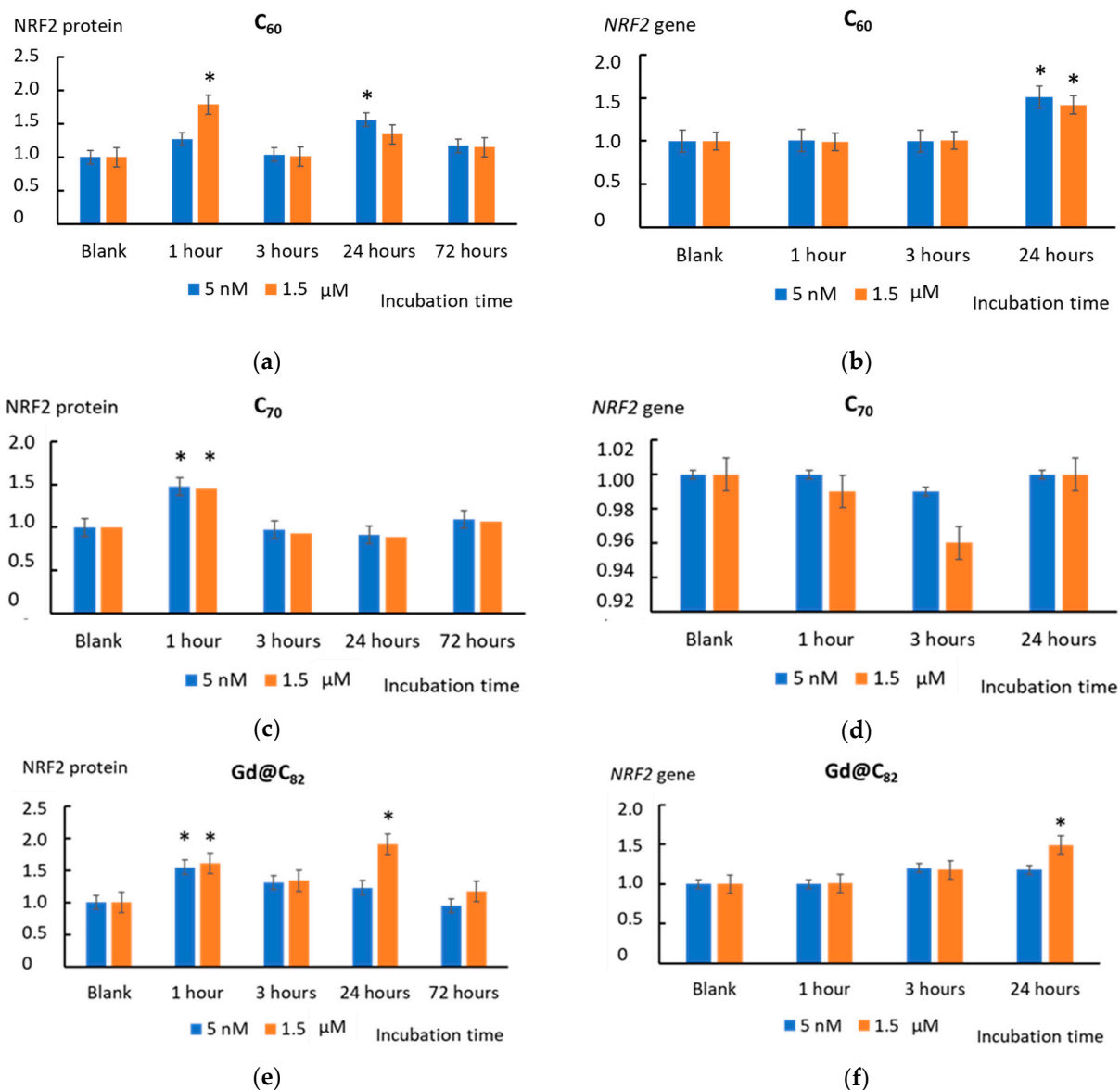


**Figure 10.** The NRF2 protein level in the cells treated with (a)  $C_{60}$ , (c)  $C_{70}$ , and (e)  $Gd@C_{82}$  at concentrations of 5 nM and 1.5 μM related to the blank cells incubated without the AFDs. The expression of the *NRF2* gene in cells incubated with (b)  $C_{60}$ , (d)  $C_{70}$ , and (f)  $Gd@C_{82}$  at concentrations of 5 nM and 1.5 μM. The *NRF2* RNA level is the mean from three replicates related to the *NRF2* gene expression in the blank cells. The *TBP* gene was used as an internal-standard gene. (\*) denotes significant differences with the blank cells,  $p < 0.01$ , a nonparametric U-test.

After 1 h of incubation, the expression of the *NRF2* gene did not increase while NRF2 protein increased. That fact indicates the activation of NRF2 that already existed in the cells. After 24 h of incubation, the expression of the *NRF2* gene increased due to incubation with  $C_{60}$  in both concentrations and  $Gd@C_{82}$  at 1.5 μM, which leads to an increase in the transcriptional activity of the *NRF2* gene in cells (Figure 10b,d,f).

### 2.9. Heme Oxygenase 1 and NAD(P)H Quinone Dehydrogenase 1

We studied the transcriptional activity of the *HO-1* gene (*HMOX1*), which encodes heme oxygenase 1 and is the target gene of the transcription factor NRF2. An increase in the expression of the *HMOX1* gene was found after 24 h of incubation with  $C_{60}$  (5 nM and 1.5  $\mu$ M) and  $Gd@C_{82}$  (1.5  $\mu$ M) ( $p < 0.01$ ). This fact is also evidence of the transcriptional activity of the *NRF2* gene in the cells (Figure 11).

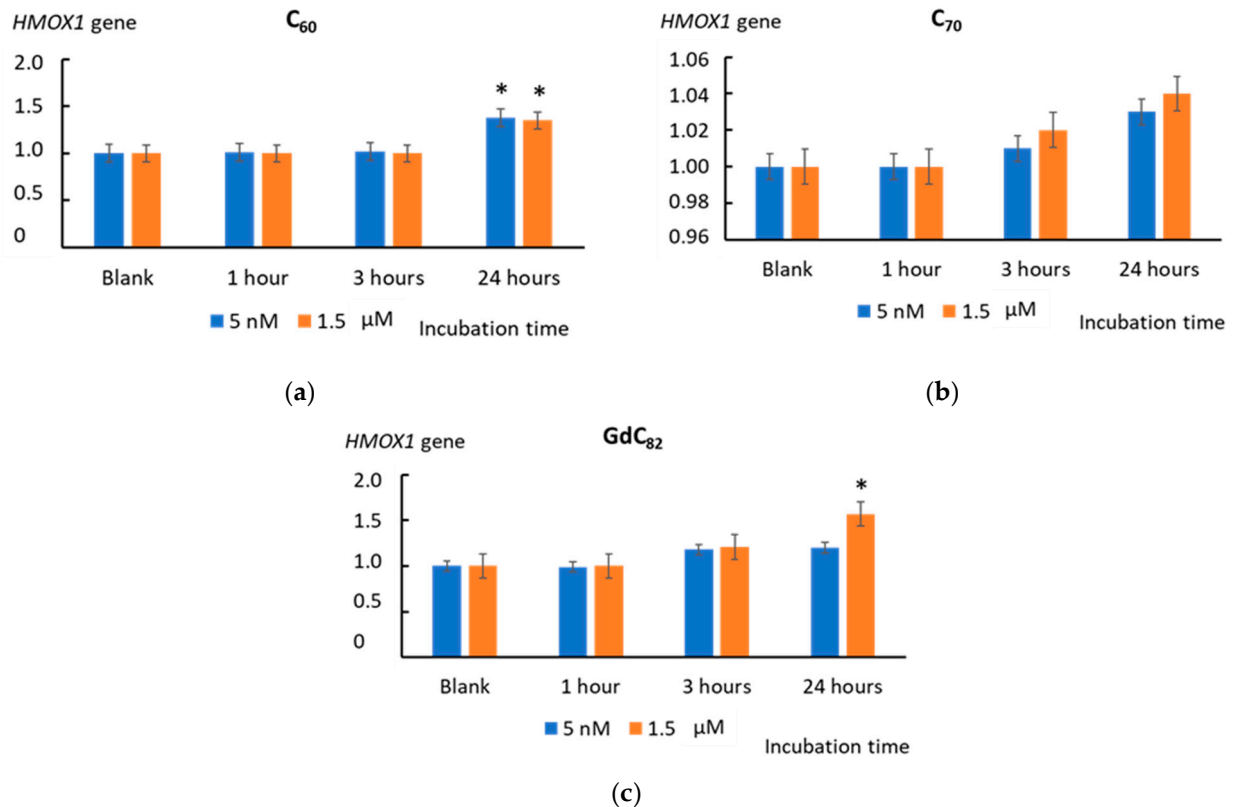


**Figure 11.** The expression of the *HMOX1* gene in cells incubated with (a)  $C_{60}$ , (b)  $C_{70}$ , and (c)  $Gd@C_{82}$  at concentrations of 5 nM and 1.5  $\mu$ M. The *HMOX1* RNA level is the mean from three replicates related to the *HMOX1* gene expression in the blank cells. The *TBP* gene was used as an internal-standard gene. (\*) denotes significant differences with the blank cells,  $p < 0.01$ , a nonparametric U-test.

The NAD(P)H quinone oxidoreductase 1 (*NQO1*) gene is also a target gene for the NRF2 transcription factor. We found an increase in the expression of the *NQO1* gene after 24 h of incubation with  $C_{60}$  (5 nM and 1.5  $\mu$ M) ( $p < 0.01$ ) and after 24 h of incubation with  $Gd@C_{82}$  (1.5  $\mu$ M) ( $p < 0.01$ ), which also confirms the activation of NRF2 in the cells (Figure 12).

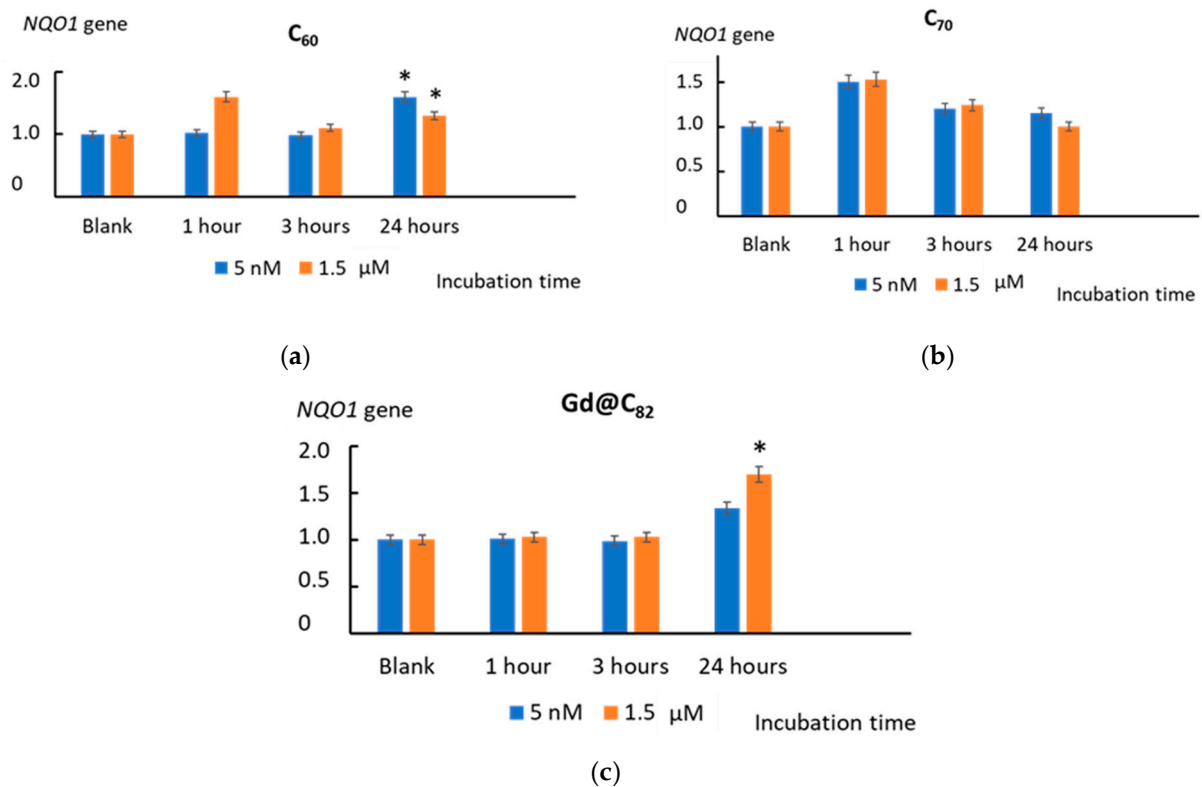


**Figure 12.** The expression of the *NQO1* gene in cells incubated with (a) *C*<sub>60</sub>, (b) *C*<sub>70</sub>, and (c) *Gd@C*<sub>82</sub> at concentrations of 5 nM and 1.5 μM. The *NQO1* RNA level is the mean from three replicates related to the *NQO1* gene expression in the blank cells. The *TBP* gene was used as an internal-standard gene. (\*) denotes significant differences with the blank cells,  $p < 0.01$ , a nonparametric U-test.

### 3. Discussion

We incubated human fetal lung fibroblasts with aqueous fullerene dispersions *C*<sub>60</sub>, *C*<sub>70</sub>, and *Gd@C*<sub>82</sub> for 1, 2, and 24 h and investigated the expression of genes and proteins of oxidative stress and anti-inflammatory response. We studied two concentrations in the nanomolar and micromolar ranges since it is known that the regulation of ROS homeostasis depends on the concentration of substances. The main results are summarized in Figure 13.

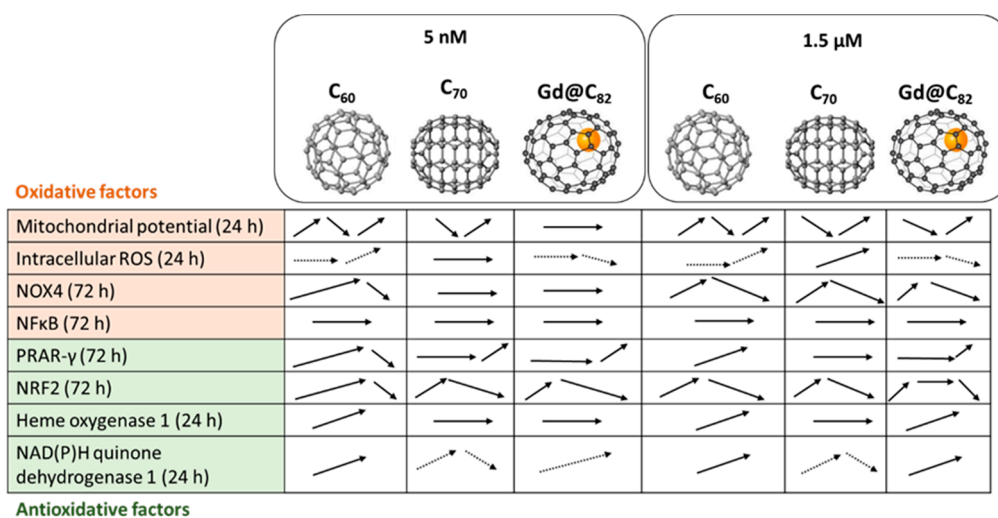


**Figure 13.** The dynamics of changes in the studied parameters over time (the time range is indicated in the first column) for two concentrations of aqueous fullerene dispersions. Solid lines denote significant changes and dashed lines, trends.

We studied two somewhat different concentrations to assess whether the effect of fullerenes on genes is monotonic or if there is a switching point. It is known that ROS-active substances exhibit pro- or antioxidant features depending on their concentration [47]. All the studied aqueous fullerene dispersions were safe for cells in a wide range of concentrations. AFDs of C<sub>60</sub> and C<sub>70</sub> did not cause cell death up to a concentration of 10 μM; however, metallofullerene Gd@C<sub>82</sub> was less safe and caused the death of 20% cells at 100-fold lower concentrations (0.1 μM). We have selected the same concentrations for all AFDs to compare their effects. Therefore, we studied 1.5 μM, the safe upper concentration for Gd@C<sub>82</sub>. A concentration of 5 nM was selected because this concentration still affects the genes and proteins.

The MTT test is commonly used to assess the metabolic activity of cells, mainly to mitochondrial functionality. Therefore, we studied the effects of AFDs on the mitochondria of HFLF cells using flow cytometry. Tetramethylrhodamine, methyl ester (TMRM), is a cell-permeant, cationic fluorescent dye that is readily sequestered by active mitochondria with intact membrane potentials. This dye is a lipophilic cation accumulated by mitochondria in proportion to ΔΨ [48,49]. The mitochondrial membrane potential is a global indicator of mitochondrial function and the metabolic state of cells. Upon loss of the mitochondrial membrane potential, TMRM accumulation will cease, and the signal will dim or disappear.

Both concentrations of C<sub>60</sub> and C<sub>70</sub> showed similar dynamics. For the first hour, C<sub>60</sub> activated mitochondria; then, their metabolism returned quickly to the initial level. A higher concentration of C<sub>60</sub> had a more significant effect. For C<sub>70</sub>, on the contrary, the metabolism was suppressed, then returned and increased by the end of the 24-h period. The metallofullerene acted similarly in a high concentration but did not affect a low concentration. The mechanism of activation of metabolism by fullerenes is challenging to explain without considering the spatial distribution of nanoparticles in the cell, which requires further microscopic experiments.

Mitochondrial respiratory chains are the primary intracellular sources of ROS because, in oxidative phosphorylation, superoxide anion radicals leak from the chain. After 24 h of incubation, C<sub>60</sub> and C<sub>70</sub> caused an increase in the activity of mitochondria. Thus, they can be considered mitochondrial “prooxidants”.

We have previously shown that concerning the superoxide anion radical fullerenes can be arranged in the row Gd@C<sub>82</sub> > C<sub>60</sub> > C<sub>70</sub> for the ability to scavenge SAR; and C<sub>60</sub> and C<sub>70</sub> differ in the mechanism of interaction with SAR from SOD, which allows them to be instead considered superoxide scavengers, in contrast to Gd@C<sub>82</sub>, which, presumably, is a SOD mimic [33]. This result is consistent with the electron affinity row C<sub>60</sub> < C<sub>70</sub> < Gd@C<sub>82</sub>. The insertion of Gd into a C<sub>82</sub> cage increases the electron affinity to 3.3 eV [50]. Moreover, the high polarizability of fullerenes facilitates the attachment of radicals to their surface [51].

As for intracellular ROS, C<sub>60</sub> and C<sub>70</sub> showed a similar trend (Figure 7a,b). After 24 h of incubation, ROS increased. However, these changes were significant for a high concentration of C<sub>70</sub>, possibly because C<sub>60</sub> is a stronger antioxidant for the superoxide anion radical. Metallofullerene is an even stronger antioxidant than C<sub>60</sub>. It also did not have an activating effect on mitochondria. Perhaps that is why, after incubation with Gd@C<sub>82</sub>, intracellular ROS decreased.

Besides mitochondrial electron transport chains, NADPH oxidases are critical sources of ROS. Trends in protein and gene expression were similar. Both concentrations of C<sub>60</sub> caused an increase in NOX4 expression. The effect of C<sub>70</sub> and Gd@C<sub>82</sub> was achieved for a higher concentration. Therefore, C<sub>60</sub> is a more active stimulus for the NOX4 system.

The studied fullerenes do not affect the NFκB, but they do affect the expression of PPAR-γ, which is sensitive to oxidized lipids [52]. C<sub>70</sub> and Gd@C<sub>82</sub> had a pronounced effect after 72 h of incubation, and C<sub>60</sub> acted much more actively in the first hours. We have previously found that C<sub>60</sub> is a very weak inducer of lipid peroxidation (unpublished data), while C<sub>70</sub> and Gd@C<sub>82</sub> at the studied concentrations did not induce lipid peroxidation. This behavior may explain the rapid increase in the expression of this gene in response to incubation with C<sub>60</sub>.

Summing up the “prooxidant part,” all studied fullerenes directly affected mitochondrial metabolism and activated NOX4, with C<sub>60</sub> having the most significant effect. Perhaps this is due to its smaller molecule size. The incubation with fullerenes led to an increase in intracellular ROS, except for Gd@C<sub>82</sub>. Perhaps this is due to the balance of its pro- and antioxidant properties. Gd@C<sub>82</sub> is a weaker prooxidant and a stronger antioxidant concerning the superoxide radical. Moreover, it exhibits SOD-like properties [33].

The development of intracellular oxidative stress leads to the activation of the NRF2 anti-inflammatory pathway. NRF2 in normal cells in the complex with the cytoskeleton protein KEAP1 is inactive. This complex lies mostly in a cytoplasm [53–55]. After modifying KEAP with ROS, NRF2 dissociates from KEAP and moves into the nucleus. In the nucleus, NRF2 reacts with ARE (antioxidant response elements) of genes, coding the enzymes for detoxication and cytoprotective proteins such as NAD(P)H quinone dehydrogenase 1 (NQO1) and heme oxygenase 1 (HO-1) [56].

The incubation of cells with all AFDs activated this pathway within one hour. C<sub>60</sub> and Gd@C<sub>82</sub> had a long-term effect of up to 24 h. The effect of C<sub>70</sub> was expressed within one hour, and no gene expression was found. An increase in the transcriptional activity of the NRF2 gene in cells is also evidenced by an increase in the transcriptional activity of the HMOX1 and NQO1 genes, which are the target genes of the NRF2 transcription factor. A significant increase in expression was obtained for C<sub>60</sub> and Gd@C<sub>82</sub>, but not for C<sub>70</sub>. Summing up the “antioxidant part”, we can say that C<sub>60</sub> and Gd@C<sub>82</sub> were more effective inducers of the anti-inflammatory pathway than C<sub>70</sub>.

Limitations. Here, we have studied the effects of aqueous fullerene dispersions on human fetal lung fibroblasts. These cells are an excellent model for studying general cell properties. We understand that studies on several lines are needed for more substantiated conclusions. Therefore, we will continue studying the effects of AFDs in mesenchymal stem cells and cancer cells.

## 4. Materials and Methods

### 4.1. AFD Preparation and Characterization

#### 4.1.1. Reagents

Pristine C<sub>60</sub> and C<sub>70</sub> (>99.5%) fullerenes were purchased from Limited Liability Scientific and Production Company NeoTechProduct (Saint Petersburg, Russia). The soot containing the Gd@C<sub>2n</sub> endohedral metal fullerenes (total content of Gd atoms up to 4 wt.% checked by ICP-OES, and the value of total Gd was recalculated to the general formula of the molecule), Gd@C<sub>82</sub> has been synthesized by the evaporation of the composite graphite electrodes compounded by gadolinium in the electric arc reactor as we previously described elsewhere [34]. Standard reference materials and quality control standards of required elements with certified values (Inorganic Ventures, Christiansburg, VA, USA) were used to conduct ICP-OES measurements. A 20 ppm (in 5 wt.% HNO<sub>3</sub>) scandium solution was used as an internal standard. Ultrapure water Milli-Q<sup>®</sup> Type (Merck, Germany) was applied during the research (total organic carbon < 3 ppb).

#### 4.1.2. Preparation of Aqueous Fullerene Dispersions by Direct Ultrasound Probe Sonication

AFDs were prepared by the direct sonication with a commercially available off-the-shelf ultrasound probe with a timer MEF93.T (LLC MELFIZ-ul'trazvuk, Moscow, Russia). Ultrasonic tip (surface areas  $0.63 \pm 0.02$  cm<sup>2</sup>) and electrical-power mode (0.6 kW) were used. Ultrasound tips were made of titanium alloys, grade TM3 (ISO 28401:2010). The weighted fullerene portion of ca. 0.05 g, 10 mL of toluene, and 50 mL of ultrapure water were subsequently added to a conical flask (250 mL). The solution was exposed to ultrasonic treatment for 12 h with a pause for 30 min every 60 min. The prepared solution was filtered through a 0.45 µm cellulose filter and diluted to the mark with 50 mL of ultrapure water.

#### 4.1.3. Characterization

Particle size distribution, electrokinetic potential  $\zeta$ , and polydispersity index were determined according to ISO 22412:2017. The results were verified using two analyzers under the same conditions. A Brookhaven Omni (Brookhaven National Lab, Upton, NY, USA) and a Malvern Zetasizer Nano ZS (Malvern Panalytical, Great Malvern, UK) were used in the 5–1000 nm size range. Measurement angles were 90°, 15°, 173° for Brookhaven Omni and 175° for Malvern Zetasizer Nano ZS.

An Agilent 720 ICP-OES spectrometer (Agilent, Santa Clara, CA, USA) with an axial view was used for elemental analysis.

MALDI MS spectra were recorded using AutoFlex II MALDI TOF/TOF mass spectrometer (Bruker Daltonics, Billerica, MA, USA). MALDI-ToF spectra were acquired by 50 shots in the positive and negative ion reflector mode with a 337-nm molecular nitrogen laser at 80% its power within a mass range from 400 to 1600–5000 Da.  $\alpha$ -Cyano-4-hydroxycinnamic acid in a mixture of 30:70 (*v/v*) acetonitrile: 0.1% trifluoroacetic acid in water was used as a matrix on an MTP 384 ground steel plate.

The analysis by IR spectroscopy was carried out on a Vertex 70 IR Fourier spectrometer (Bruker Optik GmbH, Ettingen, Germany) with a GladiATR attachment for a single attenuated total internal reflection (ATR) with a diamond crystal (Pike Technologies, Madison, WI, USA).

As we showed previously, spectrophotometry has proved itself well for estimating the concentration of fullerenes in aqueous dispersions [57]. UV/visible absorption spectra were recorded using a two-beam spectrophotometer Cary 4000 (Agilent, Santa Clara, CA, USA). Before the spectrophotometric measurements, we assessed the total non-volatile organic carbon by total organic carbon analysis, as well as other organic components using HPLC-UV or GC-MS. After the total concentration had been determined, calibration UV/visible spectra were recorded, the apparent molar absorptivities ( $\epsilon$ ) were calculated to estimate fullerene concentrations. This technique works well for conventional C<sub>60</sub> and C<sub>70</sub> fullerenes [56]. For endohedral fullerenes, we used the most express approach based on direct measurement of gadolinium in the sample by ICP-OES.

High-resolution images of the aqueous dispersions of C<sub>60</sub>, C<sub>70</sub>, and Gd@C<sub>82</sub> were obtained using a JEM 2100F field emission electron microscope (Jeol, Tokyo, Japan) with an accelerating voltage of 200 kV. For transmission electron microscopy, the aqueous fullerene dispersions were concentrated up to 200 times by ultracentrifugation at 30 krpm for 45 min at 4 °C. To increase the volatility of the solvent, 200  $\mu$ L of ethanol was added to 1.00 mL of the concentrated AFD solutions [57].

#### 4.2. Cell Culture

The Research Centre for Medical Genetics (RCMG) provided human fetal lung fibroblasts (HFLF) (the 2nd–6th cell passage). Approval#5 was obtained from the Committee for Medical and Health Research Ethics of RCMG. Cells were seeded at  $1.7 \times 10^4$  per mL in DMEM (Paneco, Moscow, Russia) with a 10% fetal calf serum (PAA Laboratories, Vienna, Austria), 50 U/mL penicillin, 50- $\mu$ g/mL streptomycin, and 10- $\mu$ g/mL gentamycin (all the reagents were from Sigma-Aldrich, St. Louis, MO, USA) and cultured at 37 °C for 2 or 24 h, as described elsewhere [19,20]. Various concentrations of AFDs were added to the cells. The cells were incubated for time intervals ranging from 1 h to 72 h.

Two cultures of the same line of HFLF were used. The data obtained were completely consistent with each other. The article presents the total results for two cultures.

#### 4.3. MTT Assay and Mitotracker Test

Cell viability was assessed with the 3-(4,5-dimethylthiazol-2-yl)-2,5-diphenyltetrazolium bromide (MTT) assay, as described previously [19,20]. Cells were incubated with AFDs in a 96-well plate for 72 h. The plates were read at 550 nm with EnSpire plate reader (EnSpire Equipment, Turku, Finland). MTT was purchased from Sigma-Aldrich, St. Louis, MO, USA.

The mitotracker test was carried out using a membrane-voltage-dependent dye, tetramethylrhodamine methyl ester (TMRM) (Thermo Fisher, Waltham, MA, USA). TMRM is a cell-permeant, cationic, red-orange fluorescent dye that is readily sequestered by active mitochondria.

#### 4.4. Reactive Oxygen Species Assays

Protein expression was assessed with flow cytometry using specific antibodies on a flow cytometer CyFlow Space (Partec, Meckenheim, Germany). Cells were washed with a Versene solution (Thermo Fisher Scientific, Waltham, MA, USA), treated with 0.25% trypsin (Paneco, Moscow, Russia), washed with the culture medium, and suspended in phosphate buffer solution (pH 7.4) (Paneco, Moscow, Russia). The cells were fixed with paraformaldehyde (PFA, Sigma-Aldrich, Saint Louis, MO, USA) at 37 °C for 10 min, then washed three times with 0.5% BSA–PBS and permeabilized with 0.1% Triton X-100 (BSA and Triton X-100 were from Sigma-Aldrich, Saint Louis, MO, USA) in PBS for 15 min at 20 °C or with 90% methanol (Sigma-Aldrich, Saint Louis, MO, USA) at 4 °C, then washed with 0.5% BSA–PBS (3 times). The cells were stained with conjugated antibodies (1 µg/mL) for 2 h at room temperature, washed with PBS, and analyzed by a flow cytometer (CytoFlex S, Beckman Coulter, Brea, CA, USA).

#### 4.5. Quantification of mRNA Levels

Gene expression was assessed by real-time polymerase chain reaction (PCR). After exposure to fullerenes, RNA was isolated from the cells using YellowSolve kits (Klonogen, St. Petersburg, Russia) according to the standard procedure, followed by phenol–chloroform extraction and precipitation with chloroform and isoamyl alcohol (49:1). The RNA concentration was determined using the Quant-iT RiboGreen RNA reagent (MoBiTec, Göttingen, Germany) on a plate reader (EnSpire equipment, Turku, Finland),  $\lambda_{\text{ex}} = 487 \text{ nm}$ ,  $\lambda_{\text{fl}} = 524 \text{ nm}$ . According to the standard procedure, the reverse transcription reaction was carried out using reagents from Sileks (Moscow, Russia). PCR was performed using the appropriate primers (Synthol) and the SYBR Green PCR Master Mix (Applied Biosystems, Foster City, CA, USA) on a StepOnePlus device (Applied Biosystems, Foster City, CA, USA). The technical error was approximately 2%. TBP was used as a reference gene.

#### 4.6. Fluorescence Microscopy

An Axio Scope.A1 microscope (Carl Zeiss, Oberkochen, Germany) was used for fluorescent microscopy of cells. The fluorescence experiments were performed in a 6-well plate at a cell concentration of  $10^6$  cells/well. No less than 100 fields of view were analyzed; fluorescence intensity per a cell and the total fluorescence were analyzed using microscope software.

#### 4.7. Statistical Analysis

Experiments were repeated in triplicate. In FCA, the medians of the signal intensities were analyzed. Figures show the mean and standard deviation (SD). The significance of the observed differences was analyzed with the nonparametric Mann–Whitney *U*-test. The *p*-values < 0.01 were considered statistically significant and marked on figures with the “\*” sign. The data were analyzed with Excel, Microsoft Office (Microsoft, Redmond, USA), Statistica 6.0 (Dell Round Rock, TX, USA), and StatGraphics (Statgraphics Technologies, The Plains, VA, USA).

## 5. Conclusions

The aqueous dispersions of C<sub>60</sub>, C<sub>70</sub>, and Gd@C<sub>82</sub> fullerenes are active participants in ROS homeostasis. Low and high concentrations of AFDs have similar effects, and we can hypothesize that these effects are monotonic within the cell viability range. The studied effects were various in strength. C<sub>70</sub> was the most inert substance, C<sub>60</sub> was the most active substance. They all have both a “prooxidant” and “antioxidant” effect, but with a different

balance. Presumably, Gd@C<sub>82</sub> was a substance with more pronounced antioxidant and anti-inflammatory properties, while C<sub>70</sub>, on the contrary, had more pronounced “prooxidant” properties. A more comprehensive understanding of the role of fullerenes will be obtained after studying their effect on DNA damage and the adaptive response (activation of repair systems, autophagy, and apoptosis), which is the aim of our subsequent studies.

**Supplementary Materials:** The following are available online at <https://www.mdpi.com/article/10.3390/ijms22116130/s1>.

**Author Contributions:** Conceptualization, E.V.P. and S.V.K.; methodology, E.V.P., M.A.P. and S.V.K.; validation, S.V.K., E.V.P. and E.S.E.; investigation, E.A.S., E.S.E., L.V.K., I.V.R. and O.A.D.; resources, I.V.M. and N.N.V.; data curation, S.V.K., E.V.P., I.V.M. and N.N.V.; writing—original draft preparation, S.V.K. and E.V.P.; writing—review and editing, S.V.K., M.A.P. and E.V.P.; visualization, N.N.V.; supervision, M.A.P. and N.N.V.; project administration, I.V.M. All authors have read and agreed to the published version of the manuscript.

**Funding:** This research was supported by the Russian Science Foundation, Project No. 19-73-00143.

**Institutional Review Board Statement:** Not applicable.

**Informed Consent Statement:** Not applicable.

**Data Availability Statement:** The datasets used and/or analyzed during the current study are available from the corresponding author on reasonable request.

**Acknowledgments:** I.E. Kareev and V.P. Bubnov provided technical support for Gd-endofullerene synthesis.

**Conflicts of Interest:** The authors declare no conflict of interest.

## References

1. Yamashita, T.; Yamashita, K.; Nabeshi, H.; Yoshikawa, T.; Yoshioka, Y.; Tsunoda, S.I.; Tsutsumi, Y. Carbon Nanomaterials: Efficacy and Safety for Nanomedicine. *Materials* **2012**, *5*, 350–363. [CrossRef]
2. Dellinger, A.; Zhou, Z.; Connor, J.; Madhankumar, A.B.; Pamujula, S.; Sayes, C.M.; Kepley, C.L. Application of fullerenes in nanomedicine: An update. *Nanomedicine* **2013**, *8*, 1191–1208. [CrossRef]
3. Partha, R.; Conyers, J.L. Biomedical applications of functionalized fullerene-based nanomaterials. *Int. J. Nanomed.* **2009**, *4*, 261–275.
4. Tagmatarchis, N.; Shinohara, H. Fullerenes in medicinal chemistry and their biological applications. *Mini Rev. Med. Chem.* **2001**, *1*, 339–348. [CrossRef]
5. Maeda, Y.; Tsuchiya, T.; Lu, X.; Takano, Y.; Akasaka, T.; Nagase, S. Current progress on the chemical functionalization and supramolecular chemistry of M@C<sub>82</sub>. *Nanoscale* **2011**, *3*, 2421–2429. [CrossRef] [PubMed]
6. Kumar, M.; Raza, K. C<sub>60</sub>-fullerenes as Drug Delivery Carriers for Anticancer Agents: Promises and Hurdles. *Pharm. Nanotechnol.* **2017**, *5*, 169–179. [CrossRef] [PubMed]
7. Luo, Z.; Xu, X.; Zhang, X.; Hu, L. Development of calixarenes, cyclodextrins and fullerenes as new platforms for anti-HIV drug design: An overview. *Mini Rev. Med. Chem.* **2013**, *13*, 1160–1165. [CrossRef] [PubMed]
8. Ghiassi, K.B.; Olmstead, M.M.; Balch, A.L. Gadolinium-containing endohedral fullerenes: Structures and function as magnetic resonance imaging (MRI) agents. *Dalton Trans.* **2014**, *43*, 7346–7358. [CrossRef]
9. Sachkova, A.S.; Kovel, E.S.; Churilov, G.N.; Guseynov, O.A.; Bondar, A.A.; Dubinina, I.A.; Kudryasheva, N.S. On mechanism of antioxidant effect of fullereneols. *Biochem. Biophys. Rep.* **2017**, *9*, 1–8. [CrossRef]
10. Injac, R.; Prijatelj, M.; Strukelj, B. Fullerene nanoparticles: Toxicity and antioxidant activity. *Methods Mol. Biol.* **2013**, *1028*, 75–100. [CrossRef] [PubMed]
11. Dugan, L.L.; Lovett, E.G.; Quick, K.L.; Lotharius, J.; Lin, T.T.; O’Malley, K.L. Fullerene-based antioxidants and neurodegenerative disorders. *Parkinsonism Relat. Disord.* **2001**, *7*, 243–246. [CrossRef]
12. Zay, S.Y.; Zavodovskiy, D.A.; Bogutskaya, K.I.; Nozdrenko, D.N.; Prylutskyy, Y.I. Prospects of C<sub>60</sub> Fullerene Application as a Mean of Prevention and Correction of Ischemic-Reperfusion Injury in the Skeletal Muscle Tissue. *Fiziol. Zh.* **2016**, *62*, 66–77. [CrossRef] [PubMed]
13. Liu, Q.; Cui, Q.; Li, X.J.; Jin, L. The applications of buckminsterfullerene C<sub>60</sub> and derivatives in orthopaedic research. *Connect. Tissue Res.* **2014**, *55*, 71–79. [CrossRef] [PubMed]
14. Lin, A.M.; Fang, S.F.; Lin, S.Z.; Chou, C.K.; Luh, T.Y.; Ho, L.T. Local carboxyfullerene protects cortical infarction in rat brain. *Neurosci. Res.* **2002**, *43*, 317–321. [CrossRef]
15. Chistyakov, V.A.; Smirnova, Y.O.; Prazdnova, E.V.; Soldatov, A.V. Possible mechanisms of fullerene C<sub>60</sub> antioxidant action. *Biomed. Res. Int.* **2013**, *2013*, 821498. [CrossRef]

16. Galvan, Y.P.; Alperovich, I.; Zolotukhin, P.; Prazdnova, E.; Mazanko, M.; Belanova, A.; Chistyakov, V. Fullerenes as Anti-Aging Antioxidants. *Curr. Aging Sci.* **2017**, *10*, 56–67. [[CrossRef](#)]
17. Li, J.; Chen, L.; Yan, L.; Gu, Z.; Chen, Z.; Zhang, A.; Zhao, F. A Novel Drug Design Strategy: An Inspiration from Encaging Tumor by Metallofullerenol Gd@C<sub>82</sub>(OH)<sub>22</sub>. *Molecules* **2019**, *24*, 2387. [[CrossRef](#)]
18. Meng, J.; Liang, X.; Chen, X.; Zhao, Y. Biological characterizations of [Gd@C<sub>82</sub>(OH)<sub>22</sub>]<sub>n</sub> nanoparticles as fullerene derivatives for cancer therapy. *Integr. Biol.* **2013**, *5*, 43–47. [[CrossRef](#)]
19. Ershova, E.S.; Sergeeva, V.; Chausheva, A.I.; Zheglo, D.G.; Nikitina, V.; Smirnova, T.D.; Kameneva, L.V.; Porokhovnik, L.N.; Kutsev, S.I.; Troshin, P.A.; et al. Toxic and DNA damaging effects of a functionalized fullerene in human embryonic lung fibroblasts. *Mutat. Res. Genet. Toxicol. Environ. Mutagenesis* **2016**, *805*, 46–57. [[CrossRef](#)]
20. Ershova, E.S.; Sergeeva, V.A.; Tabakov, V.J.; Kameneva, L.A.; Porokhovnik, L.N.; Voronov, I.I.; Khakina, E.A.; Troshin, P.A.; Kutsev, S.I.; Veiko, N.N.; et al. Functionalized Fullerene Increases NF-kappaB Activity and Blocks Genotoxic Effect of Oxidative Stress in Serum-Starving Human Embryo Lung Diploid Fibroblasts. *Oxid. Med. Cell. Longev.* **2016**, *2016*, 9895245. [[CrossRef](#)]
21. Fujita, K.; Morimoto, Y.; Ogami, A.; Myojyo, T.; Tanaka, I.; Shimada, M.; Wang, W.N.; Endoh, S.; Uchida, K.; Nakazato, T.; et al. Gene expression profiles in rat lung after inhalation exposure to C<sub>60</sub> fullerene particles. *Toxicology* **2009**, *258*, 47–55. [[CrossRef](#)]
22. Jovanovic, B.; Ji, T.; Palic, D. Gene expression of zebrafish embryos exposed to titanium dioxide nanoparticles and hydroxylated fullerenes. *Ecotoxicol. Environ. Saf.* **2011**, *74*, 1518–1525. [[CrossRef](#)] [[PubMed](#)]
23. Funakoshi-Tago, M.; Nagata, T.; Tago, K.; Tsukada, M.; Tanaka, K.; Nakamura, S.; Mashino, T.; Kasahara, T. Fullerene derivative prevents cellular transformation induced by JAK2 V617F mutant through inhibiting c-Jun N-terminal kinase pathway. *Cell. Signal.* **2012**, *24*, 2024–2034. [[CrossRef](#)]
24. Etem, E.O.; Bal, R.; Akagac, A.E.; Kuloglu, T.; Tuzcu, M.; Andrievsky, G.V.; Buran, I.; Nedzvetsky, V.S.; Baydas, G. The effects of hydrated C<sub>60</sub> fullerene on gene expression profile of TRPM2 and TRPM7 in hyperhomocysteinemic mice. *J. Recept. Signal. Transduct. Res.* **2014**, *34*, 317–324. [[CrossRef](#)]
25. Ye, S.; Chen, M.; Jiang, Y.; Chen, M.; Zhou, T.; Wang, Y.; Hou, Z.; Ren, L. Polyhydroxylated fullerene attenuates oxidative stress-induced apoptosis via a fortifying Nrf2-regulated cellular antioxidant defence system. *Int. J. Nanomed.* **2014**, *9*, 2073–2087. [[CrossRef](#)]
26. Hao, T.; Zhou, J.; Lu, S.; Yang, B.; Wang, Y.; Fang, W.; Jiang, X.; Lin, Q.; Li, J.; Wang, C. Fullerene mediates proliferation and cardiomyogenic differentiation of adipose-derived stem cells via modulation of MAPK pathway and cardiac protein expression. *Int. J. Nanomed.* **2016**, *11*, 269–283. [[CrossRef](#)]
27. Nie, X.; Tang, J.; Liu, Y.; Cai, R.; Miao, Q.; Zhao, Y.; Chen, C. Fullerenol inhibits the crosstalk between bone marrow-derived mesenchymal stem cells and tumor cells by regulating MAPK signaling. *Nanomedicine* **2017**, *13*, 1879–1890. [[CrossRef](#)] [[PubMed](#)]
28. Zhu, X.; Sollogoub, M.; Zhang, Y. Biological applications of hydrophilic C<sub>60</sub> derivatives (hC<sub>60</sub>s)-A structural perspective. *Eur. J. Med. Chem.* **2016**, *115*, 438–452. [[CrossRef](#)] [[PubMed](#)]
29. Kovel, E.S.; Sachkova, A.S.; Vnukova, N.G.; Churilov, G.N.; Knyazeva, E.M.; Kudryasheva, N.S. Antioxidant Activity and Toxicity of Fullerenols via Bioluminescence Signaling: Role of Oxygen Substituents. *Int. J. Mol. Sci.* **2019**, *20*, 2324. [[CrossRef](#)]
30. Labille, J.; Masion, A.; Ziarelli, F.; Rose, J.; Brant, J.; Villieras, F.; Pelletier, M.; Borschneck, D.; Wiesner, M.R.; Bottero, J.Y. Hydration and dispersion of C<sub>60</sub> in aqueous systems: The nature of water-fullerene interactions. *Langmuir* **2009**, *25*, 11232–11235. [[CrossRef](#)] [[PubMed](#)]
31. Mikheev, I.V.; Pirogova, M.O.; Usoltseva, L.O.; Uzhel, A.S.; Bolotnik, T.A.; Kareev, I.E.; Bubnov, V.P.; Lukonina, N.S.; Volkov, D.S.; Goryunkov, A.A.; et al. Green and rapid preparation of long-term stable aqueous dispersions of fullerenes and endohedral fullerenes: The pros and cons of an ultrasonic probe. *Ultrason. Sonochem.* **2021**, *73*, 105533. [[CrossRef](#)]
32. Mosharova, I.V.; Dallakyan, G.A.; Mikheev, I.V.; Il'inskii, V.V.; Akulova, A.Y. Changes in the Quantitative and Functional Characteristics of Bacterioplankton under the Influence of Aqueous Unmodified Fullerene capital ES, Cyrillic60 Dispersions. *Dokl. Biochem. Biophys.* **2019**, *487*, 256–259. [[CrossRef](#)]
33. Mikheev, I.V.; Sozarukova, M.M.; Proskurnina, E.V.; Kareev, I.E.; Proskurnin, M.A. Non-Functionalized Fullerenes and Endo-fullerenes in Aqueous Dispersions as Superoxide Scavengers. *Molecules* **2020**, *25*, 2506. [[CrossRef](#)]
34. Bubnov, V.P.; Laukhina, E.E.; Kareev, I.E.; Koltover, V.K.; Prokhorova, T.G.; Yagubskii, E.B.; Kozmin, Y.P. Endohedral Metallofullerenes: A Convenient Gram-Scale Preparation. *Chem. Mater.* **2002**, *14*, 1004–1008. [[CrossRef](#)]
35. Ko, W.B.; Heo, J.Y.; Nam, J.H.; Lee, K.B. Synthesis of a water-soluble fullerene [C<sub>60</sub>] under ultrasonication. *Ultrasonics* **2004**, *41*, 727–730. [[CrossRef](#)] [[PubMed](#)]
36. Taurozzi, J.S.; Hackley, V.A.; Wiesner, M. Preparation of nanoparticle dispersions from powdered material using ultrasonic disruption. *NIST Spec. Publ.* **2012**, *1200*, 1200–1202.
37. Braun, T. (Ed.) *Nuclear and Radiation Chemical Approaches to Fullerene Science*; Springer: Dordrecht, The Netherlands, 2000; Volume 1, p. 203.
38. Treubig, J.M.; Brown, P.R. Analysis of C<sub>60</sub> and C<sub>70</sub> fullerenes using high-performance liquid chromatography–Fourier transform infrared spectroscopy. *J. Chromatogr. A* **2002**, *960*, 135–142. [[CrossRef](#)]
39. Wang, J.; Li, Z.; Li, S.; Qi, W.; Liu, P.; Liu, F.; Ye, Y.; Wu, L.; Wang, L.; Wu, W. Adsorption of Cu(II) on Oxidized Multi-Walled Carbon Nanotubes in the Presence of Hydroxylated and Carboxylated Fullerenes. *PLoS ONE* **2013**, *8*, e72475. [[CrossRef](#)]
40. Cataldo, F.; Iglesias-Groth, S.; Machado, A. Low and High Temperature Infrared Spectroscopy of C<sub>60</sub> and C<sub>70</sub> Fullerenes. *Fuller. Nanotub. Carbon Nanostructures* **2010**, *18*, 224–235. [[CrossRef](#)]

41. Krause, M.; Kuran, P.; Kirbach, U.; Dunsch, L. Raman and infrared spectra of Tm@C<sub>82</sub> and Gd@C<sub>82</sub>. *Carbon* **1999**, *37*, 113–115. [[CrossRef](#)]
42. Nakagawa, Y.; Suzuki, T.; Ishii, H.; Nakae, D.; Ogata, A. Cytotoxic effects of hydroxylated fullerenes on isolated rat hepatocytes via mitochondrial dysfunction. *Arch. Toxicol.* **2011**, *85*, 1429–1440. [[CrossRef](#)]
43. Dellinger, A.; Zhou, Z.; Norton, S.K.; Lenk, R.; Conrad, D.; Kepley, C.L. Uptake and distribution of fullerenes in human mast cells. *Nanomedicine* **2010**, *6*, 575–582. [[CrossRef](#)] [[PubMed](#)]
44. Moghadam, Z.M.; Henneke, P.; Kolter, J. From Flies to Men: ROS and the NADPH Oxidase in Phagocytes. *Front. Cell Dev. Biol.* **2021**, *9*, 628991. [[CrossRef](#)]
45. Scirpo, R.; Fiorotto, R.; Villani, A.; Amenduni, M.; Spirli, C.; Strazzabosco, M. Stimulation of nuclear receptor peroxisome proliferator-activated receptor-gamma limits NF-kappaB-dependent inflammation in mouse cystic fibrosis biliary epithelium. *Hepatology* **2015**, *62*, 1551–1562. [[CrossRef](#)] [[PubMed](#)]
46. Ricote, M.; Glass, C.K. PPARs and molecular mechanisms of transrepression. *Biochim. Biophys. Acta* **2007**, *1771*, 926–935. [[CrossRef](#)] [[PubMed](#)]
47. Sies, H.; Jones, D.P. Reactive oxygen species (ROS) as pleiotropic physiological signalling agents. *Nat. Rev. Mol. Cell Biol.* **2020**, *21*, 363–383. [[CrossRef](#)] [[PubMed](#)]
48. Scaduto, R.C.; Grotyohann, L.W. Measurement of Mitochondrial Membrane Potential Using Fluorescent Rhodamine Derivatives. *Biophys. J.* **1999**, *76*, 469–477. [[CrossRef](#)]
49. Creed, S.; McKenzie, M. Measurement of Mitochondrial Membrane Potential with the Fluorescent Dye Tetramethylrhodamine Methyl Ester (TMRM). *Methods Mol. Biol.* **2019**, *1928*, 69–76. [[CrossRef](#)]
50. Boltalina, O.; Ioffe, I.; Sorokin, I.; Sidorov, L.N. Electron Affinity of Some Endohedral Lanthanide Fullerenes. *J. Phys. Chem. A* **1997**, *101*, 9561–9563. [[CrossRef](#)]
51. Ptasinska, S.; Echt, O.; Denifl, S.; Stano, M.; Sulzer, P.; Zappa, F.; Stamatovic, A.; Scheier, P.; Mark, T.D. Electron attachment to higher fullerenes and to Sc<sub>3</sub>N@C<sub>80</sub>. *J. Phys. Chem. A* **2006**, *110*, 8451–8456. [[CrossRef](#)]
52. Almeida, M.; Ambrogini, E.; Han, L.; Manolagas, S.C.; Jilka, R.L. Increased lipid oxidation causes oxidative stress, increased peroxisome proliferator-activated receptor-gamma expression, and diminished pro-osteogenic Wnt signaling in the skeleton. *J. Biol. Chem.* **2009**, *284*, 27438–27448. [[CrossRef](#)]
53. Bryan, H.K.; Olayanju, A.; Goldring, C.E.; Park, B.K. The Nrf2 cell defence pathway: Keap1-dependent and-independent mechanisms of regulation. *Biochem. Pharmacol.* **2013**, *85*, 705–717. [[CrossRef](#)] [[PubMed](#)]
54. Zhang, Y.; Xiang, Y. Molecular and cellular basis for the unique functioning of Nrf1, an indispensable transcription factor for maintaining cell homeostasis and organ integrity. *Biochem. J.* **2016**, *473*, 961–1000. [[CrossRef](#)]
55. O’Connell, M.A.; Hayes, J.D. The Keap1/Nrf2 pathway in health and disease: From the bench to the clinic. *Biochem. Soc. Trans.* **2015**, *43*, 687–689. [[CrossRef](#)] [[PubMed](#)]
56. Mikheev, I.V.; Khimich, E.S.; Rebrikova, A.T.; Volkov, D.S.; Proskurnin, M.A.; Korobov, M.V. Quasi-equilibrium distribution of pristine fullerenes C<sub>60</sub> and C<sub>70</sub> in a water–toluene system. *Carbon* **2017**, *111*, 191–197. [[CrossRef](#)]
57. Mikheev, I.V.; Usoltseva, L.O.; Ivshukov, D.A.; Volkov, D.S.; Korobov, M.V.; Proskurnin, M.A. Approach to the assessment of size-dependent thermal properties of disperse solutions: Time-resolved photothermal lensing of aqueous pristine fullerenes C<sub>60</sub> and C<sub>70</sub>. *J. Phys. Chem. C* **2016**, *120*, 28270–28287. [[CrossRef](#)]